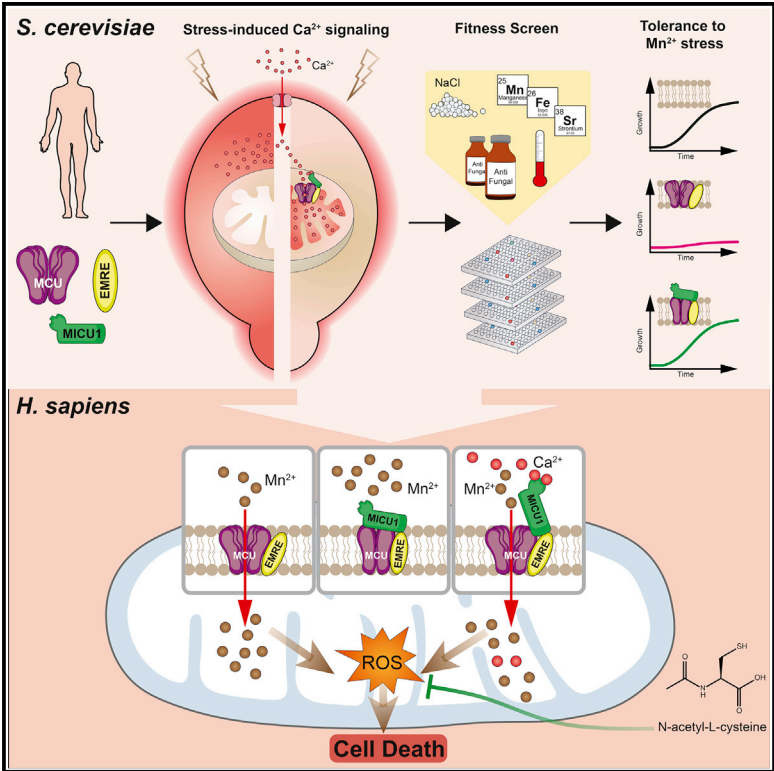


MICU1 Confers Protection from MCU-Dependent Manganese Toxicity

Graphical Abstract



Authors

Jennifer Wettmarshausen, Valerie Goh, Kai-Ting Huang, ..., Dejana Mokranjac, György Hajnóczky, Fabiana Perocchi

Correspondence

fabiana.perocchi@helmholtz-muenchen.de

In Brief

Wettmarshausen et al. develop a synthetic biology approach for *in vivo* dissection of functional interconnections between components of the mitochondrial calcium uniporter channel. They demonstrate an essential role of MICU1 in regulating MCU ion selectivity, finding that MICU1 prevents MCU-mediated Mn^{2+} overload and protects from Mn^{2+} -induced cell death.

Highlights

- MCU and MICU1 constitute the conserved unit of a eukaryotic uniporter
- Reconstitution of MCU-mediated Ca^{2+} uptake impairs yeast tolerance to Mn^{2+} stress
- MICU1 and MCU functional interaction confers a selective fitness advantage
- Loss of MICU1 hypersensitizes human cells to Mn^{2+} -dependent cell death



MICU1 Confers Protection from MCU-Dependent Manganese Toxicity

Jennifer Wettmarshausen,^{1,2,9} Valerie Goh,^{1,2,9} Kai-Ting Huang,³ Daniela M. Arduino,^{1,2} Utkarsh Tripathi,² Anja Leimpek,^{1,2} Yiming Cheng,^{1,2} Alexandros A. Pittis,^{4,5} Toni Gabaldón,^{4,5,6} Dejana Mokranjac,⁷ György Hajnóczky,³ and Fabiana Perocchi^{1,2,8,10,*}

¹Institute for Diabetes and Obesity, Helmholtz Diabetes Center (HDC), Helmholtz Zentrum München, 85764 Neuherberg, Germany

²Department of Biochemistry, Gene Center Munich, Ludwig-Maximilians Universität München, 81377 Munich, Germany

³Department of Pathology, Anatomy, and Cell Biology, MitoCare Center, Thomas Jefferson University, Philadelphia, PA 19107, USA

⁴Bioinformatics and Genomics Programme, Centre for Genomic Regulation (CRG), 08003 Barcelona, Spain

⁵Departament de Ciències Experimentals I de La Salut, Universitat Pompeu Fabra (UPF), 08003 Barcelona, Spain

⁶Institució Catalana de Recerca i Estudis Avançats (ICREA), 08010 Barcelona, Spain

⁷Biomedical Center Munich - Physiological Chemistry, Ludwig-Maximilians Universität München, 82152 Martinsried, Germany

⁸Munich Cluster for Systems Neurology, 81377 Munich, Germany

⁹These authors contributed equally

¹⁰Lead Contact

*Correspondence: fabiana.perocchi@helmholtz-muenchen.de

<https://doi.org/10.1016/j.celrep.2018.10.037>

SUMMARY

The mitochondrial calcium uniporter is a highly selective ion channel composed of species- and tissue-specific subunits. However, the functional role of each component still remains unclear. Here, we establish a synthetic biology approach to dissect the interdependence between the pore-forming subunit MCU and the calcium-sensing regulator MICU1. Correlated evolutionary patterns across 247 eukaryotes indicate that their co-occurrence may have conferred a positive fitness advantage. We find that, while the heterologous reconstitution of MCU and EMRE *in vivo* in yeast enhances manganese stress, this is prevented by co-expression of MICU1. Accordingly, MICU1 deletion sensitizes human cells to manganese-dependent cell death by disinhibiting MCU-mediated manganese uptake. As a result, manganese overload increases oxidative stress, which can be effectively prevented by NAC treatment. Our study identifies a critical contribution of MICU1 to the uniporter selectivity, with important implications for patients with MICU1 deficiency, as well as neurological disorders arising upon chronic manganese exposure.

INTRODUCTION

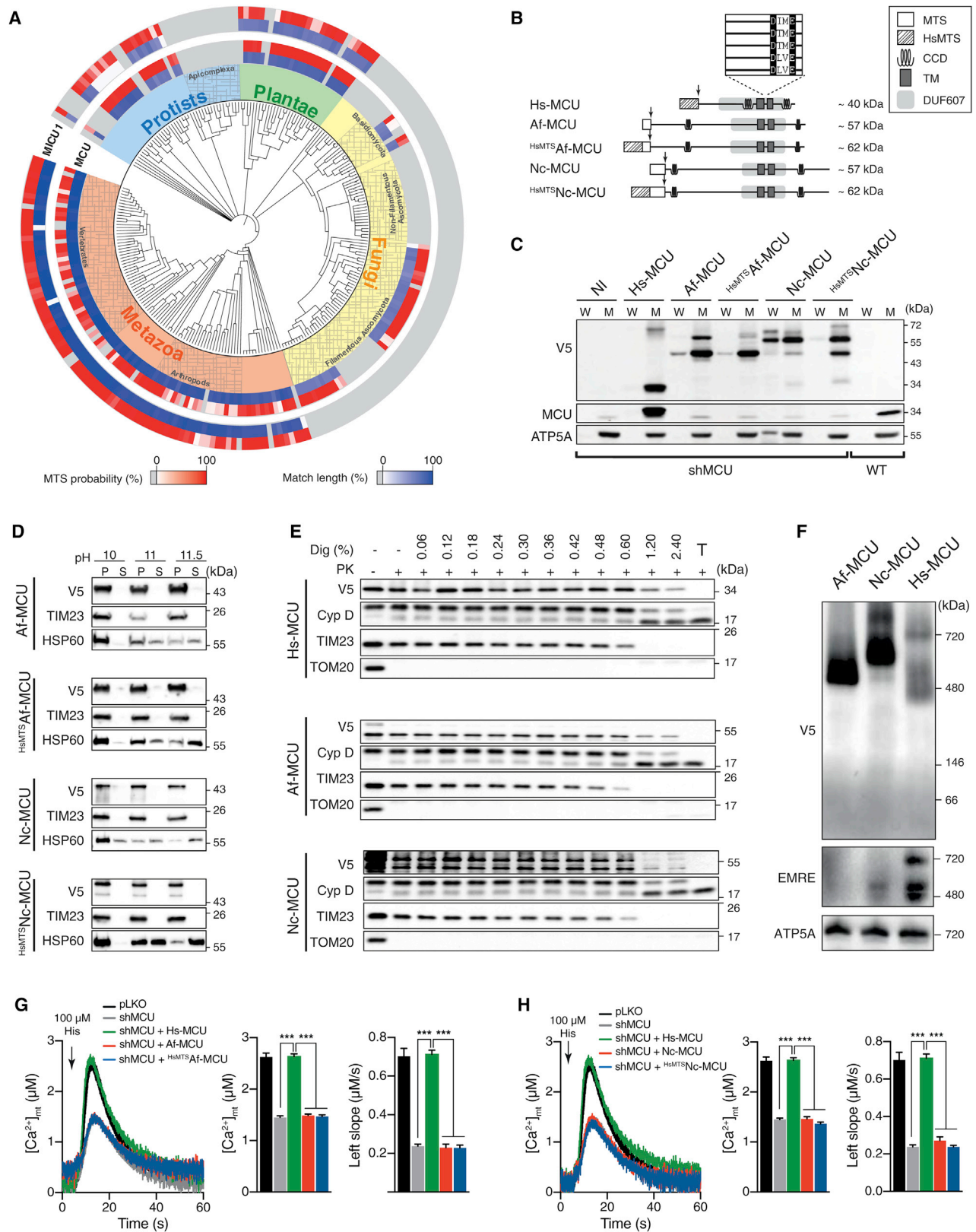
Mitochondria from several organisms are able to regulate intracellular calcium (Ca^{2+}) dynamics due to their ability to rapidly and transiently uptake Ca^{2+} . This occurs through an electrophoretic uniporter mechanism that makes use of the steep electrochemical gradient generated by the respiratory chain (Carafoli and Lehninger, 1971; Deluca and Engstrom, 1961; Vasington

and Murphy, 1962) and is mediated by a highly selective Ca^{2+} channel located at the inner mitochondrial membrane (Kirichok et al., 2004). However, the molecular identity of the mitochondrial Ca^{2+} uniporter has remained a mystery for decades. Recently, a functional genomics approach has allowed the discovery of the first peripheral Ca^{2+} -dependent regulator (MICU1) (Perocchi et al., 2010) and the transmembrane pore-forming subunit of the uniporter (MCU) (Baughman et al., 2011; De Stefani et al., 2011), paving the way for the identification of several other inhibitory and enhancing effectors of mitochondrial Ca^{2+} (mt-Ca^{2+}) uptake such as MCUB, MICU2, MICU3, and EMRE (De Stefani et al., 2016).

Overall, the complex molecular nature of the mammalian uniporter highlights the physiological relevance of achieving great plasticity and selectivity in mt-Ca^{2+} uptake. Due to the presence of a very large driving force for cation influx, the uniporter must at the same time limit mt-Ca^{2+} accumulation when the cell is at rest to prevent vicious Ca^{2+} cycling and rapidly transmit a cytosolic Ca^{2+} (cyt-Ca^{2+}) signal to the mitochondrial matrix during signaling. The highly selective permeability of the uniporter for Ca^{2+} is thought to derive from the high-affinity binding of the ion to the DXE motif at the MCU pore (Arduino et al., 2017; Baughman et al., 2011; Cao et al., 2017; Chaudhuri et al., 2013; Oxenoid et al., 2016), whereas both gating and cooperative activation of the uniporter have been attributed to its interaction with hetero-oligomers of MICU1 and MICU2 or MICU3 (Csordás et al., 2013; Kamer et al., 2017; Mallilankaraman et al., 2012; Patron et al., 2014, 2018). However, the respective functional and mechanistic roles of those subunits in regulating uniporter activity have been thus far investigated in mammalian systems, in which the interpretation of results is hampered by differences in the degree of gene silencing, tissue-specific protein composition (Murgia and Rizzuto, 2015; Vecellio Reane et al., 2016), stoichiometry, and compensatory remodeling (Liu et al., 2016; Paillard et al., 2017) of the channel.

The budding yeast *Saccharomyces cerevisiae* represents an ideal testbed for dissecting the functional contribution of each





(legend on next page)

component of the human uniporter, given that it completely lacks any detectable MCU homolog (Bick et al., 2012; Cheng and Perocchi, 2015) and endogenous mt-Ca²⁺ transport activity (Arduino et al., 2017; Carafoli and Lehninger, 1971; Kovács-Bogdán et al., 2014; Yamamoto et al., 2016), while enabling the facile expression and targeting of human mitochondrial proteins. Moreover, we and others have shown that mt-Ca²⁺ uptake can be readily reconstituted *in vitro* in isolated yeast mitochondria by co-expressing the human MCU and EMRE subunits (Arduino et al., 2017; Kovács-Bogdán et al., 2014; Yamamoto et al., 2016). Here, we establish a yeast-based heterologous system to investigate the functional interconnection between MCU and MICU1 *in vivo*. By screening for stress conditions whereby the expression of MICU1 in an MCU-reconstituted yeast strain would confer a fitness advantage, we identify a protective role of MICU1 against MCU-dependent manganese (Mn²⁺) toxicity. Consistent with these findings, human HEK293 cells lacking MICU1 become permeable to Mn²⁺, whose uptake is genetically and chemically prevented by the re-introduction of wild-type (WT) MICU1 and by ruthenium red (RuRed), respectively. As a consequence, MICU1 knockout (KO) cells are greatly sensitized to Mn²⁺-induced cell death that is triggered by an increase in oxidative stress and prevented by *N*-acetyl-L-cysteine (NAC) treatment. Our findings highlight a previously unknown role of MICU1 in regulating the selectivity of the uniporter, with potential implications for both MICU1 and Mn²⁺-related human disorders.

RESULTS

Phylogenetic Profiling of MCU and MICU1 across 247 Eukaryotes

We examined the co-evolution and predicted mitochondrial co-localization of MCU and MICU1 across 247 fully sequenced eukaryotic species (Figure 1A) from multiple taxonomic levels at different evolutionary distances to maximize the resolution of coupled evolutionary patterns (see also <https://itol.embl.de/tree/774755176425021526503446>) (Cheng and Perocchi, 2015). We found that MCU homologs were widely distributed in all of the major eukaryotic groups, present in nearly all Metazoa and Plantae, but only in some Protozoa (e.g., *Trypanosoma cruzi*, *Leishmania major*) and few Fungi. Instead, they apparently had been lost in all Apicomplexa (e.g., *Plasmodium falciparum*), mitochondrial-devoid, single-cell eukaryotes (e.g., *Entamoeba histolytica*, *Giardia lamblia*, *E. cuniculi*), and Saccharomycota (e.g., *S. cerevisiae*, *Schizosaccharomyces pombe*, *Candida*

glabrata). We observed a largely overlapping distribution of MICU1 and MCU homologs, pointing to a strong functional association between the two proteins, which we now know to be part of the same complex. Only a few species within Basidiomycota and Ascomycota fungal clades, such as *Neurospora crassa* and *Aspergillus fumigatus*, contained MCU-like proteins without any detectable MICU1 orthologs.

Given that Fungi also lack EMRE (Sancak et al., 2013), we reasoned that fungal MCU homologs should be self-sufficient to drive mt-Ca²⁺ uptake, similarly to the MCU ortholog from *Dicostillium discoideum* (Dd-MCU) (Arduino et al., 2017; Kovács-Bogdán et al., 2014). Therefore, we analyzed their ability to complement MCU loss of function in human cells. We expressed *A. fumigatus* (Af-MCU), *N. crassa* (Nc-MCU), or human MCU (Hs-MCU) with a C-terminal V5 tag in MCU knockdown (shMCU) HeLa cells (Figure 1B). To ensure the targeting of fungal MCUs to human mitochondria, we also tested chimera proteins consisting of the Hs-MCU mitochondrial targeting sequence (HsMTS) fused to the full-length form of Nc-MCU (^{HsMTS}Nc-MCU) and Af-MCU (^{HsMTS}Af-MCU). We showed that all constructs were properly localized (Figure 1C) and inserted (Figure 1D) into the inner mitochondrial membrane of shMCU HeLa cells, with the C termini facing the matrix side, similar to Hs-MCU (Figure 1E). Furthermore, on a native gel, both Af-MCU and Nc-MCU formed a large protein complex of a size comparable to that of cells expressing Hs-MCU (Figure 1F). Next, we quantified mt-Ca²⁺ uptake transients in intact (Figures 1G and 1H) and digitonin-permeabilized (Figure S1) shMCU HeLa cells expressing Hs-MCU, Af-MCU, or Nc-MCU, together with a mitochondrial matrix-targeted WT aequorin (mt-AEQ) as a Ca²⁺ sensor. Although the expression of Hs-MCU fully rescued mt-Ca²⁺ uptake, neither Af-MCU nor Nc-MCU, with and without HsMTS, were able to functionally complement Hs-MCU loss of function.

The strong co-evolution of MCU and MICU1, together with the apparent lack of functional MCU homologs in *A. fumigatus*, *N. crassa*, and several other fungal species (Baradaran et al., 2018) that do not express any MICU1-like component, suggest that MCU and MICU1 constitute the conserved unit of a eukaryotic uniporter, and their functional interaction could be required to provide a fitness advantage.

In Vivo Reconstitution of Mitochondrial Calcium Uptake in Yeast

Yeast uses cyt-Ca²⁺ signaling to activate pro-survival, adaptive responses to diverse environmental stresses (Cyert, 2003). We

Figure 1. Evolutionary Analysis of MCU and MICU1 across 247 Eukaryotes

- (A) Phylogenetic distribution of MCU and MICU1 homologs (blue, percentage of amino acids match length). MTS, mitochondrial targeting sequence.
 (B) Schematic of ectopically expressed fungal MCU constructs and protein domains. DXXE motif and MTS cleavage site prediction (arrow) are also shown. CCD, coiled-coil domain; TM, transmembrane domain.
 (C) Analysis of whole-cell (W) and mitochondrial (M) fractions from pLKO (WT) or shMCU HeLa cells stably expressing human (Hs-MCU), *N. crassa* (Nc-MCU), or *A. fumigatus* (Af-MCU) MCU fused to a C-terminal V5-tag. HsMTS, mitochondrial targeting sequence of human MCU; NI, not infected.
 (D) Analysis of mitochondrial soluble (S) and membrane pellet (P) fractions.
 (E) Analysis of fungal MCU protein topology by proteinase K (PK) treatment. Dig, digitonin; T, triton (1%).
 (F) Macromolecular protein complex analysis of fungal MCU constructs by blue native (BN)-PAGE.
 (G and H) Representative traces and quantification of mt-Ca²⁺ transients in pLKO (WT) or shMCU HeLa cells stably expressing MCU from human (Hs-MCU) and *A. fumigatus* (Af-MCU) (G) or *N. crassa* (Nc-MCU) (H) upon histamine (His) stimulation.
 All data represent means ± SEMs; n = 6–8; ***p < 0.001, one-way ANOVA with Tukey's multiple comparisons test.
 See also Figure S1.

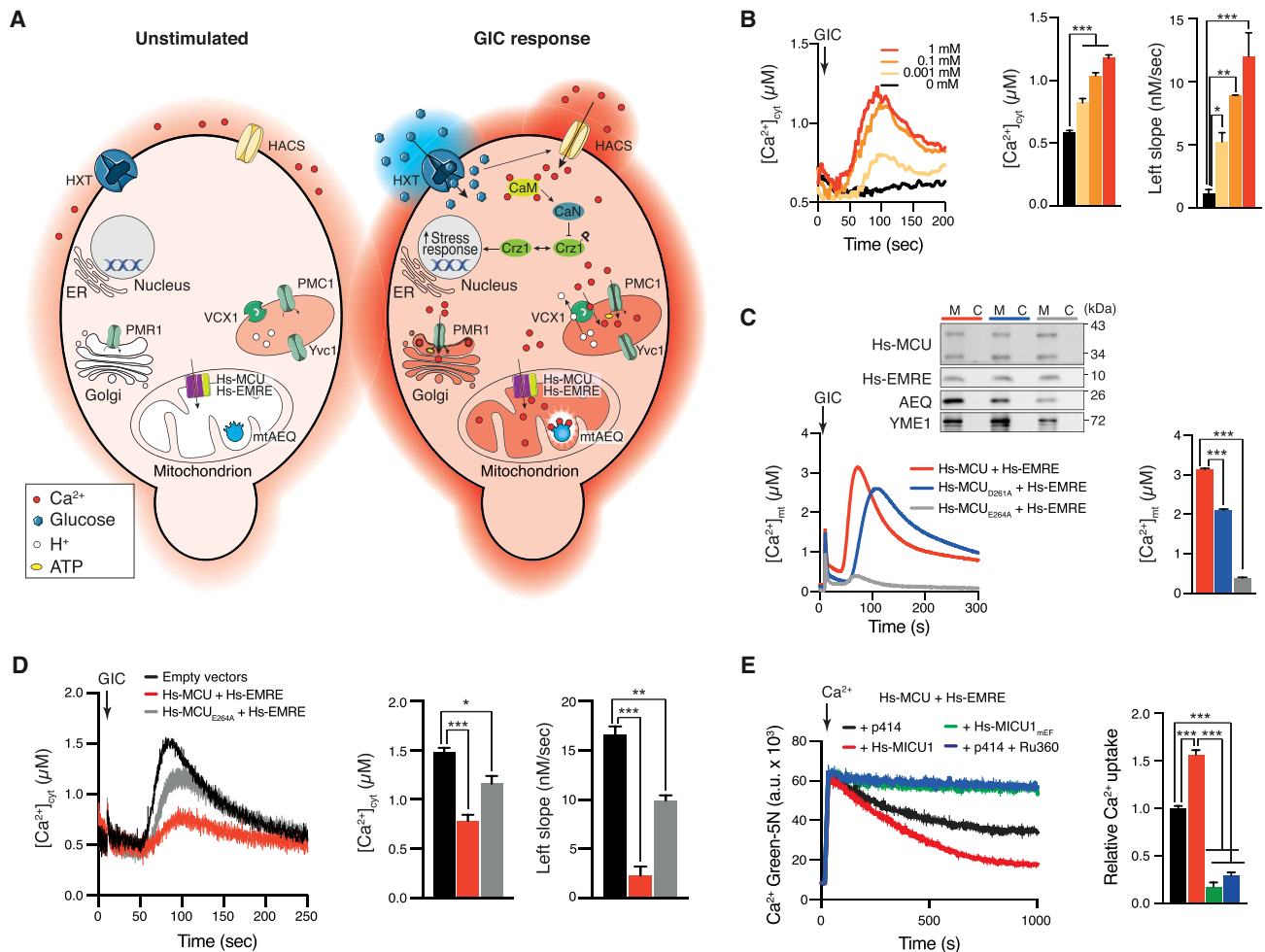


Figure 2. *In vivo* Reconstitution of mt- Ca^{2+} Uptake in Yeast

(A) Schematic of the Ca^{2+} homeostasis system and glucose-induced calcium (GIC) signaling in *S. cerevisiae*. CaM, calmodulin; CaN, calcineurin; Crz1, calcineurin-dependent transcription factor; Crz1^P, phosphorylated Crz1; ER, endoplasmic reticulum; HACs, high-affinity Ca^{2+} transport system; HXT, hexose transporter; mtAEQ, mitochondria-targeted aequorin; PMC1, vacuolar Ca^{2+} -ATPase; PMR1, ER/Golgi Ca^{2+} -ATPase; VCX1, vacuolar H^+ / Ca^{2+} exchanger; Yvc1, transient receptor potential cation (TRPC)-type Ca^{2+} channel.

(B) Cyt- Ca^{2+} transients in yeast cells upon GIC stimulation in the presence of different extracellular CaCl_2 concentrations (n = 3); *p < 0.05, **p < 0.01, ***p < 0.001; one-way ANOVA with Dunnett's multiple comparisons test.

(C) Mt- Ca^{2+} transients in yeast cells expressing WT mtAEQ, Hs-EMRE, and either WT or mutated Hs-MCU upon GIC stimulation in the presence of 1 mM CaCl_2 (n = 3); ***p < 0.0001; one-way ANOVA with Tukey's multiple comparisons test. Inset: immunoblot analysis of cytosolic (C) and mitochondrial (M) fractions.

(D) Cyt- Ca^{2+} transients in yeast cells expressing empty vectors (p425, p423) or Hs-EMRE with either WT or mutant Hs-MCU upon GIC stimulation in the presence of 1 mM CaCl_2 (n = 3); *p < 0.05, **p < 0.01, ***p < 0.001; one-way ANOVA with Dunnett's multiple comparisons test.

(E) Extracellular Ca^{2+} clearance by mitochondria isolated from the yeast strains expressing Hs-MCU, Hs-EMRE, and either an empty vector (p414), human WT MICU1 (Hs-MICU1), or EF-hands mutant MICU1 (Hs-MICU1_{mEF}), (n = 3); ***p < 0.001; one-way ANOVA with Tukey's multiple comparisons test.

All data represent means \pm SEMs.

See also Figure S2.

therefore asked whether the reconstitution of MCU-mediated mt- Ca^{2+} uptake in yeast would affect the activation of cyt- Ca^{2+} dynamics *in vivo*. As an extracellular stimulus, we chose glucose-induced calcium (GIC) activation, whereby the addition of glucose and extracellular Ca^{2+} to cells starved for >2 hr in hexose-free medium triggers cyt- Ca^{2+} transients (Figures 2A and 2B) (Groppi et al., 2011). Next, we generated yeast strains expressing WT mt-AEQ together with Hs-MCU, Hs-EMRE, or

both and confirmed that their co-expression was necessary and sufficient to drive mt- Ca^{2+} uptake *in vivo* (Figure S2A) and to respond to a wide dynamic range of external Ca^{2+} concentrations (Figure S2B). Accordingly, Hs-MCU mutants in highly conserved acidic residues within the DXE motif (Hs-MCU_{D261A}; Hs-MCU_{E264A}) were either partially functional (Hs-MCU_{D261A}) or almost completely unable (Hs-MCU_{E264A}) to fully transfer GIC-induced cyt- Ca^{2+} signals into the mitochondrial matrix

(Figure 2C). Likewise, yeast strains expressing Af-MCU or Nc-MCU (Figure S2C) were unable to drive Ca^{2+} uptake in the organelle, compared to cells reconstituted with Dd-MCU (Figure S2D). As hypothesized, the *in vivo* reconstitution of MCU-mediated mt- Ca^{2+} uptake resulted in a prompt buffering of GIC-induced cyt- Ca^{2+} elevations (Figure 2D). We then tested whether the expression of WT human MICU1 (Hs-MICU1) (Figure S2E) would be sufficient to reconstitute a Ca^{2+} -regulated uniporter in yeast. Similar to mammalian cells (Csordás et al., 2013; Kamer et al., 2017; Mallilankaraman et al., 2012), the presence of WT but not EF-hands mutant (Hs-MICU1_{mEF}) significantly increased the MCU-dependent mt- Ca^{2+} level upon GIC activation in intact cells (Figure S2F) and a bolus of high Ca^{2+} in isolated mitochondria (Figure 2E).

These results validate our *in vivo*, heterologous experimental system for the study of uniporter-mediated Ca^{2+} uptake. They also demonstrate that the expression of Hs-MCU, Hs-EMRE, and Hs-MICU1 in yeast is sufficient to reconstitute Ca^{2+} -regulated uniporter activity in response to physiological stimuli that activate intracellular Ca^{2+} signaling.

MCU Impairs Yeast Tolerance to Metal Stress

We then searched for biological conditions in which the reconstitution of MCU-mediated mt- Ca^{2+} uptake in the absence of the regulatory subunit MICU1 would lead to fitness impairment. We compared the fitness of yeast strains expressing a functional (Hs-MCU/EMRE) or an inactive (Hs-MCU_{E264A}/EMRE) uniporter to that of WT cells upon different environmental stresses (Figure 3), including heat shock, fungicide treatment, high salt, and heavy metals. To this end, we used growth rate as a proxy for cell survival and proliferation and ensured their reliance on functional mitochondria by using lactate as a non-fermentable carbon source. Overall, we observed comparable doubling times among the three different strains during normal growth at 30°C in lactate medium, which was >2-fold higher upon heat shock (37°C) (Figure 3A). Likewise, treatment with increasing doses of two antifungal drugs, miconazole and amiodarone, either decreased the growth rate of the yeast cultures by >2-fold (miconazole, 100 ng/mL) (Figure 3B) or resulted in a complete cessation of growth (amiodarone, 20 μM) (Figure 3C), regardless of the genetic background. The three strains also showed similar sensitivities to salt stress (NaCl and CaCl_2) within the range of the tested concentrations (Figures 3D, 3E, and S3A).

Instead, we observed notable differences among strains in their responses to heavy metals-induced stress (Sr^{2+} , Cu^{2+} , Zn^{2+} , Fe^{2+} , Mn^{2+}) (Figure 3F). Those cations are essential for normal growth and metabolism when present at minimal levels in the medium, but at high concentrations they can induce cytotoxicity (Wysocki and Tamás, 2010). Accordingly, with the exception of Sr^{2+} (Figure S3B), the doubling time of WT yeast cultures was >2-fold higher in the presence of high extracellular concentrations of CuCl_2 , FeCl_2 , and ZnCl_2 (Figure 3F). While all strains showed a similar tolerance to CuCl_2 and ZnCl_2 , we observed a greater hypersensitivity of the functional MCU-reconstituted strain to both Fe^{2+} and Mn^{2+} toxicity, which manifested as a drastic reduction in cell proliferation at concentrations >10 and 1 mM, respectively (Figure 3F). In addition, expression of Hs-MCU_{E264A} did not impair tolerance to Mn^{2+}

stress, whereas the same mutation was not sufficient to prevent Fe^{2+} -induced toxicity, suggesting a potentially different coordination of Fe^{2+} with the DXXE motif.

These observations indicate that in the absence of MICU1, MCU may mediate the cytotoxic accumulation of heavy metals in mitochondria.

MICU1 Protects Human Cells from MCU-Dependent Mn^{2+} Toxicity

We speculate that the co-occurrence of MCU and MICU1 could confer an evolutionary advantage by shielding mitochondria from an unwanted accumulation of heavy metals. Thus, we tested whether the reconstitution of an MICU1-regulated uniporter would be sufficient to protect yeast cells from MCU-dependent Mn^{2+} and Fe^{2+} stresses. We found that the expression of either Hs-MICU1 or Hs-MICU1_{mEF} significantly rescued the hypersensitivity of the MCU-reconstituted strain toward both Fe^{2+} (Figure S4A) and Mn^{2+} (Figure 4A) stresses. This finding indicated that MICU1 interaction with Hs-MCU and Hs-EMRE, rather than functional EF-hands, was required to prevent Fe^{2+} and Mn^{2+} entry into mitochondria, most probably by keeping the channel in a close conformation.

Next, we recapitulated the above findings in mammalian cells. To this end, we compared the viability of WT and MICU1-KO HEK293 cells upon treatment with increasing concentrations of either FeCl_2 or MnCl_2 for 48 hr. Unlike yeast, neither WT nor MICU1-KO HEK293 cells showed an increased sensitivity to Fe^{2+} treatment (Figure S4B), even at high non-physiological concentrations, indicating major differences in the mechanisms used by fungal and mammalian cells to regulate Fe^{2+} homeostasis and cope with its overload (Philpott, 2012). Instead, we observed a dramatic decrease in cell viability when MICU1-KO cells were treated with concentrations of Mn^{2+} >10 μM , which did not affect WT cells (Figure 4B). As observed in yeast, the protective role of MICU1 toward Mn^{2+} toxicity was not dependent on having functional Ca^{2+} -sensing domains, as a genetic rescue with either Hs-MICU1 or Hs-MICU1_{mEF} resulted in a significantly higher tolerance than MICU1-KO cells to 25 μM Mn^{2+} (Figures S4C and S4D).

These results pointed toward a critical role of MICU1 in inhibiting MCU-dependent Mn^{2+} toxicity, which could be exerted by directly regulating Mn^{2+} entry through the uniporter. We therefore measured mitochondrial Mn^{2+} uptake in WT and MICU1-KO HEK293 cells by monitoring the quenching of the fluorescence signal from mitochondrial compartmentalized Fura-FF upon Mn^{2+} entry in the mitochondrial matrix (Csordás and Hajnóczky, 2003). We confirmed previous findings showing that in the presence of submicromolar cyt- Ca^{2+} levels, mitochondria from WT cells are not permeable to Mn^{2+} (Figure 4C). Instead, in the same conditions, MICU1 KO cells displayed robust mitochondrial Mn^{2+} uptake, as indicated by the time-dependent quenching of the fluorescence signal upon addition of 20 μM Mn^{2+} (Figure 4C). This uptake was completely inhibited by RuRed and fully rescued by the expression of WT MICU1 in the HEK293 KO genetic background (Figure 4D), validating that the observed Mn^{2+} transport was mediated by MCU. Moreover, we showed that the pre-addition of 30 μM Ca^{2+} , a concentration at which the uniporter is disinhibited, resulted in Mn^{2+} entry also

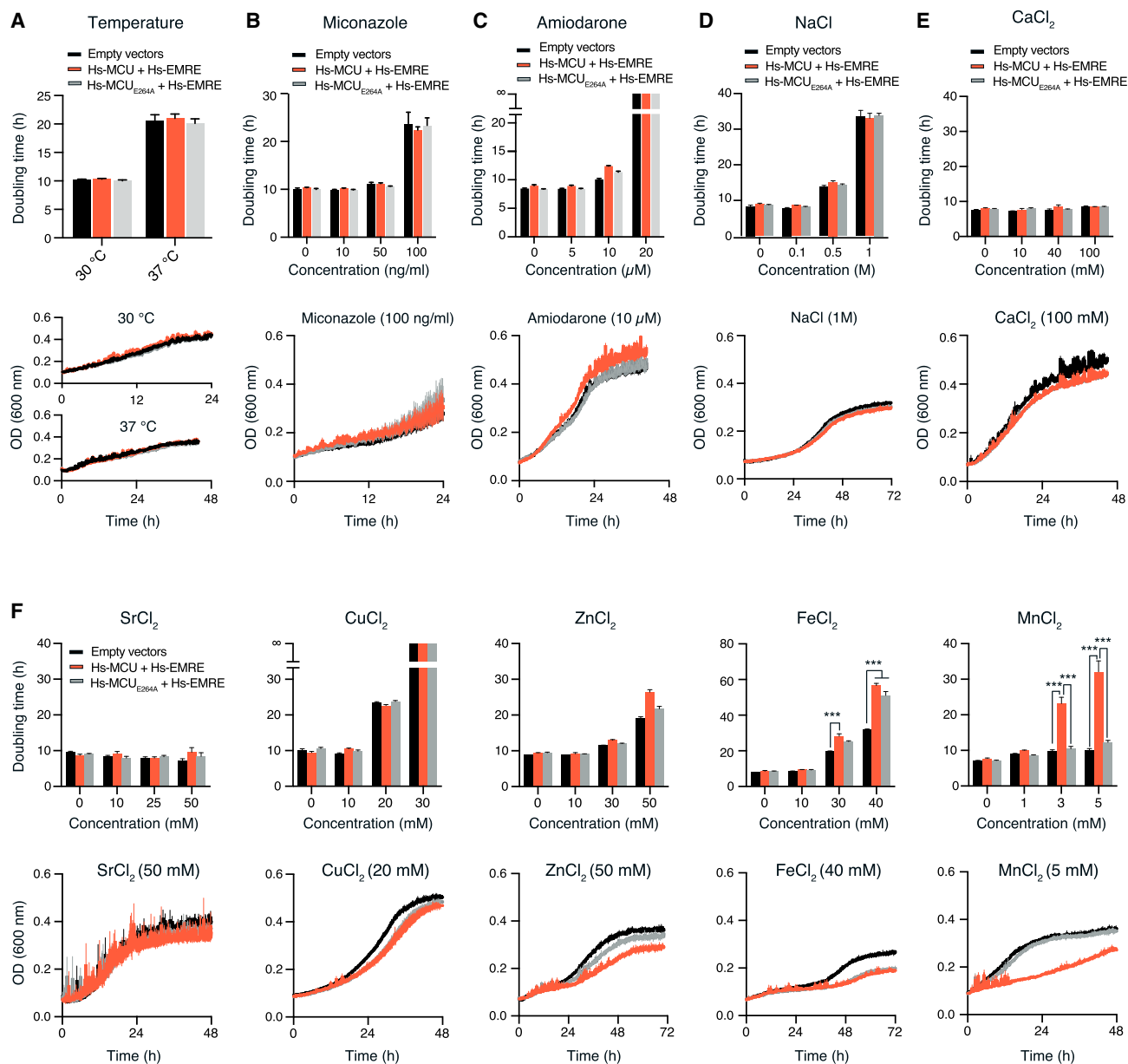


Figure 3. MCU Impairs Yeast Tolerance to Iron and Manganese Stresses

(A–F) Quantification of growth rate and average growth curve of yeast strains expressing empty vectors (p423 and p425) or Hs-EMRE with WT or mutated Hs-MCU at 30°C and 37°C (A), and at increasing concentrations of miconazole (B), amiodarone (C), NaCl (D), CaCl₂ (E), or heavy metals (F).

Data represent means ± SEMs; n = 4; ***p < 0.0001; one-way ANOVA with Tukey's multiple comparisons test.

See also Figure S3.

in HEK293 WT cells (Figure 4E), which is consistent with previous results in rat basophilic leukemia (RBL)-2H3 mast cells (Csordás and Hajnóczky, 2003).

Although the mechanism of mitochondrial Mn²⁺ toxicity is not entirely understood, it is believed that increased oxidative stress triggered by Mn²⁺ overload plays a role in the induction of cell death (Smith et al., 2017). Thus, we measured reactive oxygen species (ROS) production in MICU1-KO cells exposed to high extracellular Mn²⁺ concentrations. As shown in Figure 4F,

MICU1-KO cells exhibited a significant increase in intracellular ROS production upon 25 µM Mn²⁺ treatment, which is comparable to the level induced by treatment with H₂O₂. We then searched for strategies that could prevent Mn²⁺-induced toxicity. Fe²⁺ supplementation has already been proposed as a therapeutic strategy to treat or prevent neurological disorders due to a chronic increase of Mn²⁺ level in the blood (O'Neal and Zheng, 2015; Tai et al., 2016), as both cations compete for the same plasma membrane divalent metal transporter.

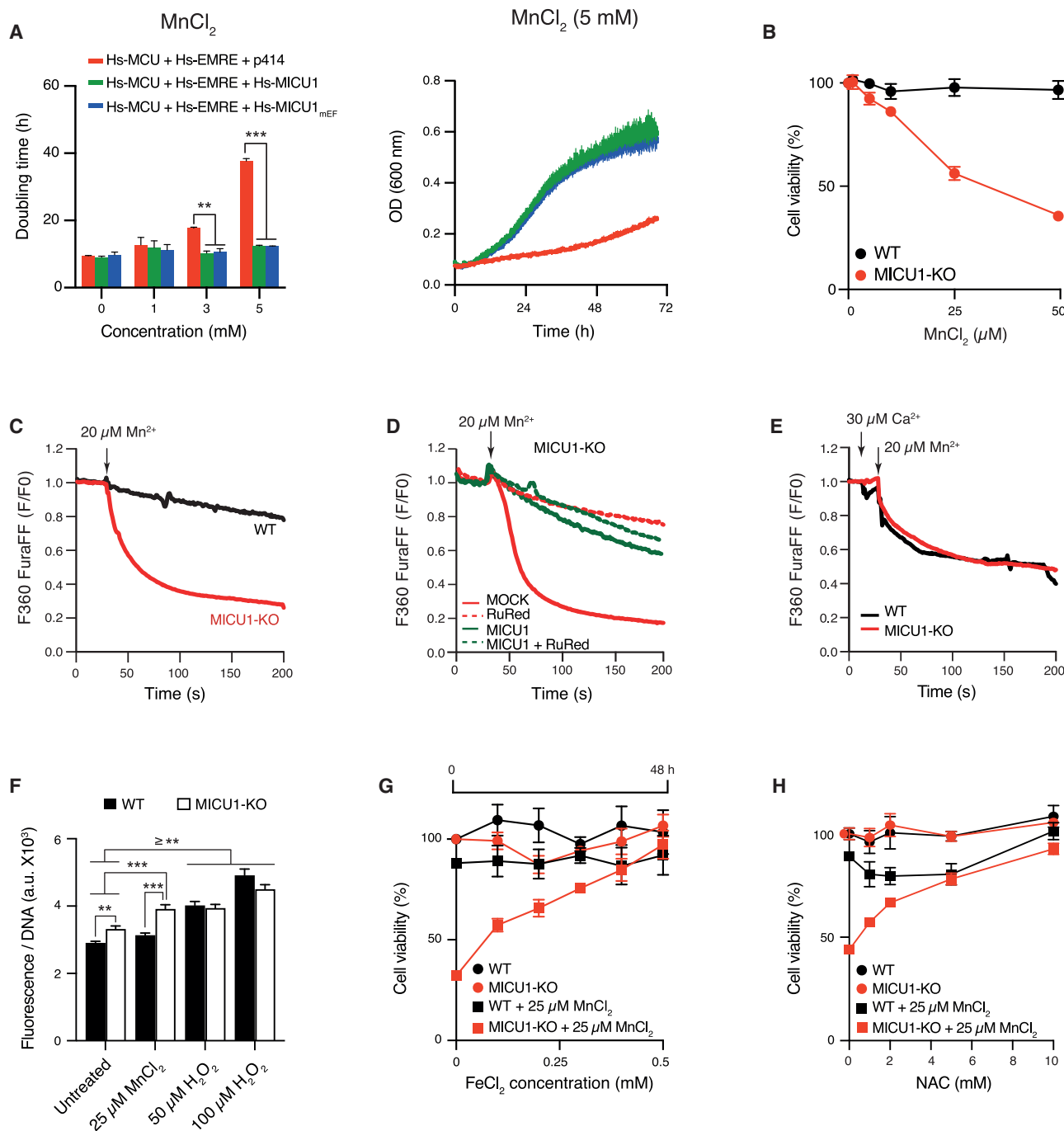


Figure 4. MICU1 Protects from Manganese-Induced Cell Death

(A) Quantification of growth rate and average growth curve of yeast strains treated with $MnCl_2$; n = 4; **p < 0.01; ***p < 0.001; one-way ANOVA with Tukey's multiple comparisons test.

(B) Cell viability of wild-type (WT) and MICU1 knockout (MICU1-KO) HEK293 cells treated for 48 hr with $MnCl_2$; n = 4.

(C–E) Detection of mitochondrial Mn^{2+} uptake through the quench of compartmentalized Fura-FF in permeabilized single WT and MICU1-KO cells in the absence (C) or presence (D) of $CaCl_2$ and upon transfection with MICU1 or pcDNA in the absence and presence of 3 μM RuRed (E). Each trace represents the mean of 40–50 cells from one of three different cell cultures.

(F) Measurements of ROS by 5-(and-6)-chloromethyl-2', 7'-dichlorodihydrofluorescein diacetate (CM-H₂DCFDA) in WT and MICU1-KO cells treated for 48 hr with vehicle, $MnCl_2$, or H_2O_2 . Data represent means \pm SEMs; n = 8; **p < 0.01, ***p < 0.001; one-way ANOVA with Tukey's multiple comparisons test.

(legend continued on next page)

Treatment of MICU1-KO cells with 25 μM Mn^{2+} in the presence of 0.5 mM FeCl_2 (Figure 4G) consistently resulted in cell survival, whereas FeCl_2 pre-treatment for 24 hr was unable to confer protection to Mn^{2+} -induced stress (Figure S4E). We also tested the effect of several antioxidant compounds on Mn^{2+} -induced oxidative stress (Figure S4F) and found that NAC treatment was able to fully rescue Mn^{2+} -induced cell death in MICU1 KO cells (Figure 4H).

Our findings establish an essential role of MICU1 in regulating the permeability of the uniporter to Mn^{2+} , which is essential for preventing Mn^{2+} -induced cytotoxicity.

DISCUSSION

Our phylogenetic analysis (Figure 1) and a previous comparative genomics study (Bick et al., 2012) highlight a widespread co-occurrence of MCU and MICU1 across Metazoa, Plantae, and Protozoa, with the exception of Fungi. The presence of MCU homologs in several Ascomycota and Basidiomycota fungal clades devoid of any detectable MICU1 has led to the hypothesis that MCU could exist independently of a Ca^{2+} -sensing regulator. This is based on the assumption that fungal MCU homologs are able per se to mediate mt- Ca^{2+} uptake, with properties similar to the mammalian uniporter. Our results from functional complementation analyses in human shMCU cells (Figures 1 and S1) and from *in vivo* reconstitution in yeast (Figure S2) show that MCU orthologs from *N. crassa* and *A. fumigatus* are unable to drive mt- Ca^{2+} uptake, despite proper expression, mitochondrial localization, topology, and assembly. Those findings are consistent with previous observations from Carafoli and Lehninger (1971) and from Gonçalves et al. (2015) that mitochondria of *N. crassa* have a limited ability to accumulate Ca^{2+} , which occurs in the range of hours, are only partially inhibited by Ru360, and are not driven by membrane potential. Recently, it was reported that a putative MCU ortholog could mediate Ca^{2+} transport into *A. fumigatus* mitochondria (Song et al., 2016) and the structures of MCU orthologs from several Fungi (Baradaran et al., 2018; Fan et al., 2018; Nguyen et al., 2018), including *N. crassa* (Yoo et al., 2018), have been characterized. However, Af-MCU-KO elicited only a 50% decrease in Ca^{2+} uptake into *A. fumigatus* mitochondria. Moreover, there is currently no direct evidence that MCU orthologs from *Nassarius fischeri* (Nguyen et al., 2018), *Fusarium graminearum*, and *Metarhizium acridum* (Fan et al., 2018) mediate mt- Ca^{2+} uptake in those organisms, neither that other fungal MCUs can reconstitute mt- Ca^{2+} uptake when expressed in yeast or mammalian cells (Baradaran et al., 2018). These results would lead to conjecture that either the MCU-like sequences found in some Fungi encode for proteins that have lost Ca^{2+} uptake ability or they could be involved in Ca^{2+} transport through mechanisms that are different from the mammalian uniporter. Further experiments will be neces-

sary to uncover the function of those MCU-like proteins in Fungi and to resolve the paradox of species with MCU-like sequences without MICU1 orthologs.

To investigate the direct contribution of MICU1 to the uniporter activity, we used the yeast *S. cerevisiae* as a model system. Previous results, including ours, have shown that Hs-MCU and Hs-EMRE are sufficient to drive Ca^{2+} uptake *in vitro* into the matrix of isolated mitochondria (Arduino et al., 2017; Kovács-Bogdán et al., 2014; Yamamoto et al., 2016). Here, we show that they can reconstitute mt- Ca^{2+} entry *in vivo* in yeast in response to a physiological increase in cyto- Ca^{2+} (Figure 2). Furthermore, similar to mammalian cells, the expression of Hs-MICU1 in MCU-reconstituted yeast cells exerts a synergistic effect on mt- Ca^{2+} uptake, which is dependent on its Ca^{2+} -sensing domains. Therefore, we searched for biological conditions whereby a positive MCU-MICU1 genetic interaction would provide a selective fitness advantage over a yeast strain reconstituted with MCU without its regulator (Figure 3). We found that MCU-reconstituted yeast cells are more susceptible to the increase of Mn^{2+} levels in the extracellular medium, which is likely due to its permeation across the uniporter (Cao et al., 2017; Csordás and Hajnóczky, 2003; Mela and Chance, 1968; Romslo and Flatmark, 1973; Saris, 2012; Vinogradov and Scarpa, 1973). Co-expression with MICU1 conferred full protection against uniporter-dependent Mn^{2+} toxicity (Figure 4), regardless of functional EF-hand domains. All of these findings were recapitulated in HEK293 cells, where the KO of MICU1 hypersensitized cells to Mn^{2+} -dependent cell death. Thus, unlike Ca^{2+} , the binding of Mn^{2+} to EF-hands (Senguen and Grabarek, 2012; Shirran and Barran, 2009) would be insufficient to trigger in MICU1 the conformational change needed for the opening of the MCU channel, a hypothesis that was recently validated by Kamer et al. (2018).

Our findings are of great relevance for patients with MICU1 loss-of-function mutations (Lewis-Smith et al., 2016; Logan et al., 2014; Musa et al., 2018). So far, the disease phenotypes observed in human patients and recapitulated in MICU1-KO mice (Antony et al., 2016; Liu et al., 2016) were attributed to high basal mt- Ca^{2+} levels, possibly due to the loss of MICU1-dependent gatekeeping of the uniporter. In light of our results, those could also result from Mn^{2+} accumulation in mitochondria, which would have an additive effect: it would increase mt- Ca^{2+} levels by inhibiting both Na^+ -dependent and Na^+ -independent mt- Ca^{2+} efflux routes (Gavin et al., 1990), and it would increase oxidative stress and trigger cell death (Smith et al., 2017). Accordingly, antioxidant treatment with NAC fully prevented Mn^{2+} -induced cell death in MICU1-KO cells. This result is consistent with previous findings showing that treatment of cells, mice, rats, and nonhuman primates with NAC during exposure to high doses of MnCl_2 is protective against Mn^{2+} cytotoxicity (Smith et al., 2017). Finally, our findings also suggest MICU1 as a possible target for neurological diseases related to chronic

(G) Cell viability of WT and MICU1-KO cells treated for 48 hr with MnCl_2 in the presence of FeCl_2 ($n = 3$).

(H) Cell viability of WT and MICU1-KO cells treated for 48 hr with MnCl_2 in the presence of *N*-acetyl-L-cysteine (NAC) ($n = 3$).

All data represent means \pm SEMs and are reported as the percentage of viable cells in untreated samples.

See also Figure S4.

exposure to environmental sources of Mn^{2+} such as, for example, Mn^{2+} -rich foods, Mn^{2+} aerosols and dusts in mines and smelters, and air pollution from the combustion of gasoline containing methylcyclopentadienyl Mn^{2+} tricarbonyl (O'Neal and Zheng, 2015).

In summary, our study demonstrates the power of combining comparative genomics analyses with the use of yeast as a model system for dissecting the functional and mechanistic role of each component of the mammalian uniporter. The reconstitution of an MICU1-regulated uniporter in yeast offers an incomparable advantage over similar investigations of MICU1 and MCU interdependence in mammalian cells, in which MICU1 KO or knock-down also has confounding effects on the expression of other uniporter subunits, such as MICU2 and MICU3 (Patron et al., 2014, 2018; Plovanich et al., 2013). Importantly, we unraveled a key role of MICU1 in regulating the selectivity of the uniporter towards Ca^{2+} ions, with important implications for patients with MICU1 deficiency.

STAR★METHODS

Detailed methods are provided in the online version of this paper and include the following:

- KEY RESOURCES TABLE
- CONTACT FOR REAGENT AND RESOURCE SHARING
- EXPERIMENTAL MODEL AND SUBJECT DETAILS
 - Cell lines
 - Yeast Strains
- METHOD DETAILS
 - Phylogenetic Profiling of MICU1 and MCU
 - Protein Domains
 - Plasmids and Reagents
 - Isolation of Crude Mitochondria from HeLa Cells
 - Topology Analysis of Mitochondrial Proteins
 - Blue Native – PAGE Analysis
 - Measurements of Mitochondrial Calcium Uptake in Intact HeLa Cells
 - Measurements of Mitochondrial Calcium Uptake in Digitonin-Permeabilized HeLa Cells
 - Subcellular Fractionation of Yeast Cells
 - Measurements of Calcium Transients in Intact Yeast Cells
 - Measurements of Mitochondrial Calcium Uptake in Isolated Yeast Mitochondria
 - Yeast Growth Measurement
 - Cell Viability Analysis
 - Mitochondrial Mn^{2+} Transport Measurement in Human Cells
 - ROS Measurement
- QUANTIFICATION AND STATISTICAL ANALYSIS
 - Quantification of Calcium Transients
 - Data Analysis

SUPPLEMENTAL INFORMATION

Supplemental Information includes four figures and can be found with this article online at <https://doi.org/10.1016/j.celrep.2018.10.037>.

ACKNOWLEDGMENTS

We acknowledge support from the German Research Foundation (DFG) under the Emmy Noether Programme (PE 2053/1-1 to F.P. and J.W.), the Munich Center for Systems Neurology (SyNergy EXC 1010 to F.P.), the Juniorverbund in der Systemmedizin "mitOmics" (FKZ 01ZX1405B to V.G. and A.L.), The Bert L & N Kuggie Vallee Foundation (to F.P. and D.M.A.), the DFG (MO1944/1-2 to D.M.), the Spanish Ministry of Economy, Industry, and Competitiveness (MEIC; BFU2015-67107), the European Union's Horizon 2020 research and innovation program under grant agreement ERC-2016-724173 (to T.G. and A.A.P.), and the NIH (RO1 GM102724 to G.H.).

AUTHOR CONTRIBUTIONS

Conceptualization, F.P.; Methodology, F.P., V.G., J.W., K.-T.H., D.M., T.G., and G.H.; Validation, V.G., J.W., K.-T.H., U.T., and A.L.; Formal Analysis, V.G., J.W., K.-T.H., A.A.P., D.M.A., and Y.C.; Investigation, V.G., J.W., and K.-T.H.; Resources, F.P., D.M., G.H., and T.G.; Writing - Original Draft, F.P., V.G., and J.W.; Writing - Review & Editing, F.P., T.G., D.M., G.H., and D.M.A.; Visualization, F.P., V.G., J.W., K.-T.H., and G.H.; Supervision, F.P., G.H. and T.G.; Funding Acquisition, F.P., D.M., T.G., and G.H.

DECLARATION OF INTERESTS

The authors declare no competing interests.

Received: June 30, 2018

Revised: August 9, 2018

Accepted: October 8, 2018

Published: November 6, 2018

REFERENCES

- Antony, A.N., Paillard, M., Moffat, C., Juskeviciute, E., Correnti, J., Bolon, B., Rubin, E., Csordás, G., Seifert, E.L., Hoek, J.B., and Hajnóczky, G. (2016). MICU1 regulation of mitochondrial Ca^{2+} uptake dictates survival and tissue regeneration. *Nat. Commun.* 7, 10955.
- Arduino, D.M., Wettmarshausen, J., Vais, H., Navas-Navarro, P., Cheng, Y., Leimpek, A., Ma, Z., Delrio-Lorenzo, A., Giordano, A., Garcia-Perez, C., et al. (2017). Systematic identification of MCU modulators by orthogonal inter-species chemical screening. *Mol. Cell* 67, 711–723.e7.
- Baradaran, R., Wang, C., Siliciano, A.F., and Long, S.B. (2018). Cryo-EM structures of fungal and metazoan mitochondrial calcium uniporters. *Nature* 559, 580–584.
- Baughman, J.M., Perocchi, F., Girgis, H.S., Plovanich, M., Belcher-Timme, C.A., Sancak, Y., Bao, X.R., Strittmatter, L., Goldberger, O., Bogorad, R.L., et al. (2011). Integrative genomics identifies MCU as an essential component of the mitochondrial calcium uniporter. *Nature* 476, 341–345.
- Bick, A.G., Calvo, S.E., and Mootha, V.K. (2012). Evolutionary diversity of the mitochondrial calcium uniporter. *Science* 336, 886.
- Bonora, M., Giorgi, C., Bononi, A., Marchi, S., Patergnani, S., Rimessi, A., Rizzuto, R., and Pinton, P. (2013). Subcellular calcium measurements in mammalian cells using jellyfish photoprotein aequorin-based probes. *Nat. Protoc.* 8, 2105–2118.
- Cao, C., Wang, S., Cui, T., Su, X.-C., and Chou, J.J. (2017). Ion and inhibitor binding of the double-ring ion selectivity filter of the mitochondrial calcium uniporter. *Proc. Natl. Acad. Sci. USA* 114, E2846–E2851.
- Carafoli, E., and Lehninger, A.L. (1971). A survey of the interaction of calcium ions with mitochondria from different tissues and species. *Biochem. J.* 122, 681–690.
- Chaudhuri, D., Sancak, Y., Mootha, V.K., and Clapham, D.E. (2013). MCU encodes the pore conducting mitochondrial calcium currents. *eLife* 2, e00704.
- Cheng, Y., and Perocchi, F. (2015). ProtPhylo: identification of protein-phenotype and protein-protein functional associations via phylogenetic profiling. *Nucleic Acids Res.* 43, W160–W168.

- Csordás, G., and Hajnóczky, G. (2003). Plasticity of mitochondrial calcium signaling. *J. Biol. Chem.* **278**, 42273–42282.
- Csordás, G., Golenár, T., Seifert, E.L., Kamer, K.J., Sancak, Y., Perocchi, F., Moffat, C., Weaver, D., de la Fuente Perez, S., Bogorad, R., et al. (2013). MICU1 controls both the threshold and cooperative activation of the mitochondrial Ca^{2+} uniporter. *Cell Metab.* **17**, 976–987.
- Cyert, M.S. (2003). Calcineurin signaling in *Saccharomyces cerevisiae*: how yeast go crazy in response to stress. *Biochem. Biophys. Res. Commun.* **311**, 1143–1150.
- De Stefani, D., Raffaello, A., Teardo, E., Szabò, I., and Rizzuto, R. (2011). A forty-kilodalton protein of the inner membrane is the mitochondrial calcium uniporter. *Nature* **476**, 336–340.
- De Stefani, D., Rizzuto, R., and Pozzan, T. (2016). Enjoy the trip: calcium in mitochondria back and forth. *Annu. Rev. Biochem.* **85**, 161–192.
- Deluca, H.F., and Engstrom, G.W. (1961). Calcium uptake by rat kidney mitochondria. *Proc. Natl. Acad. Sci. USA* **47**, 1744–1750.
- Fan, C., Fan, M., Orlando, B.J., Fastman, N.M., Zhang, J., Xu, Y., Chambers, M.G., Xu, X., Perry, K., Liao, M., and Feng, L. (2018). X-ray and cryo-EM structures of the mitochondrial calcium uniporter. *Nature* **559**, 575–579.
- Gavin, C.E., Gunter, K.K., and Gunter, T.E. (1990). Manganese and calcium efflux kinetics in brain mitochondria. Relevance to manganese toxicity. *Biochem. J.* **266**, 329–334.
- Gonçalves, A.P., Cordeiro, J.M., Monteiro, J., Lucchi, C., Correia-de-Sá, P., and Videira, A. (2015). Involvement of mitochondrial proteins in calcium signaling and cell death induced by staurosporine in *Neurospora crassa*. *Biochim. Biophys. Acta* **1847**, 1064–1074.
- Groppi, S., Belotti, F., Brandão, R.L., Martegani, E., and Tisi, R. (2011). Glucose-induced calcium influx in budding yeast involves a novel calcium transport system and can activate calcineurin. *Cell Calcium* **49**, 376–386.
- Kamer, K.J., and Mootha, V.K. (2014). MICU1 and MICU2 play non redundant roles in the regulation of the mitochondrial calcium uniporter. *EMBO Rep* **15**, 299–307.
- Kamer, K.J., Grabarek, Z., and Mootha, V.K. (2017). High-affinity cooperative Ca^{2+} binding by MICU1-MICU2 serves as an on-off switch for the uniporter. *EMBO Rep.* **18**, 1397–1411.
- Kamer, K.J., Sancak, Y., Fomina, Y., Meisel, J.D., Chaudhuri, D., Grabarek, Z., and Mootha, V.K. (2018). MICU1 imparts the mitochondrial uniporter with the ability to discriminate between Ca^{2+} and Mn^{2+} . *Proc. Natl. Acad. Sci. USA* **115**, E7960–E7969.
- Kirchok, Y., Krapivinsky, G., and Clapham, D.E. (2004). The mitochondrial calcium uniporter is a highly selective ion channel. *Nature* **427**, 360–364.
- Kovács-Bogdán, E., Sancak, Y., Kamer, K.J., Plovanich, M., Jambhekar, A., Huber, R.J., Myre, M.A., Blower, M.D., and Mootha, V.K. (2014). Reconstitution of the mitochondrial calcium uniporter in yeast. *Proc. Natl. Acad. Sci. USA* **111**, 8985–8990.
- Lewis-Smith, D., Kamer, K.J., Griffin, H., Childs, A.M., Pysden, K., Titov, D., Duff, J., Pyle, A., Taylor, R.W., Yu-Wai-Man, P., et al. (2016). Homozygous deletion in MICU1 presenting with fatigue and lethargy in childhood. *Neurol. Genet.* **2**, e59.
- Liu, J.C., Liu, J., Holmström, K.M., Menazza, S., Parks, R.J., Fergusson, M.M., Yu, Z.X., Springer, D.A., Halsey, C., Liu, C., et al. (2016). MICU1 serves as a molecular gatekeeper to prevent in vivo mitochondrial calcium overload. *Cell Rep.* **16**, 1561–1573.
- Logan, C.V., Szabadkai, G., Sharpe, J.A., Parry, D.A., Torelli, S., Childs, A.M., Kriek, M., Phadke, R., Johnson, C.A., Roberts, N.Y., et al.; UK10K Consortium (2014). Loss-of-function mutations in MICU1 cause a brain and muscle disorder linked to primary alterations in mitochondrial calcium signaling. *Nat. Genet.* **46**, 188–193.
- Mallilankaraman, K., Doonan, P., Cárdenas, C., Chandramoorthy, H.C., Müller, M., Miller, R., Hoffman, N.E., Gandhirajan, R.K., Molgó, J., Birnbaum, M.J., et al. (2012). MICU1 is an essential gatekeeper for MCU-mediated mitochondrial Ca^{2+} uptake that regulates cell survival. *Cell* **151**, 630–644.
- Mela, L., and Chance, B. (1968). Spectrophotometric measurements of the kinetics of Ca^{2+} and Mn^{2+} accumulation in mitochondria. *Biochemistry* **7**, 4059–4063.
- Mumberg, D., Müller, R., and Funk, M. (1995). Yeast vectors for the controlled expression of heterologous proteins in different genetic backgrounds. *Gene* **156**, 119–122.
- Murgia, M., and Rizzuto, R. (2015). Molecular diversity and pleiotropic role of the mitochondrial calcium uniporter. *Cell Calcium* **58**, 11–17.
- Musa, S., Eyaid, W., Kamer, K., Ali, R., Al-Mureikhi, M., Shahbeck, N., Al-Mesaifri, F., Makhseed, N., Mohamed, Z., AlShehhi, W.A., et al. (2018). A Middle Eastern founder mutation expands the genotypic and phenotypic spectrum of mitochondrial MICU1 deficiency: a report of 13 patients. *JIMD Rep.* Published online May 3, 2018. https://doi.org/10.1007/8904_2018_107.
- Nguyen, N.X., Armache, J.P., Lee, C., Yang, Y., Zeng, W., Mootha, V.K., Cheng, Y., Bai, X.C., and Jiang, Y. (2018). Cryo-EM structure of a fungal mitochondrial calcium uniporter. *Nature* **559**, 570–574.
- O’Neal, S.L., and Zheng, W. (2015). Manganese toxicity upon overexposure: a decade in review. *Curr. Environ. Health Rep.* **2**, 315–328.
- Oxenoid, K., Dong, Y., Cao, C., Cui, T., Sancak, Y., Markhard, A.L., Grabarek, Z., Kong, L., Liu, Z., Ouyang, B., et al. (2016). Architecture of the mitochondrial calcium uniporter. *Nature* **533**, 269–273.
- Paillard, M., Csordás, G., Szanda, G., Golenár, T., Debattisti, V., Bartok, A., Wang, N., Moffat, C., Seifert, E.L., Spät, A., and Hajnóczky, G. (2017). Tissue-specific mitochondrial decoding of cytoplasmic Ca^{2+} signals is controlled by the stoichiometry of MICU1/2 and MCU. *Cell Rep.* **18**, 2291–2300.
- Patron, M., Checchetto, V., Raffaello, A., Teardo, E., Vecellio Reane, D., Mantoan, M., Granatiero, V., Szabò, I., De Stefani, D., and Rizzuto, R. (2014). MICU1 and MICU2 finely tune the mitochondrial Ca^{2+} uniporter by exerting opposite effects on MCU activity. *Mol. Cell* **53**, 726–737.
- Patron, M., Granatiero, V., Espino, J., Rizzuto, R., and De Stefani, D. (2018). MICU3 is a tissue-specific enhancer of mitochondrial calcium uptake. *Cell Death Differ.* Published online May 3, 2018. <https://doi.org/10.1038/s41418-018-0113-8>.
- Perocchi, F., Gohil, V.M., Girgis, H.S., Bao, X.R., McCombs, J.E., Palmer, A.E., and Mootha, V.K. (2010). MICU1 encodes a mitochondrial EF hand protein required for Ca^{2+} uptake. *Nature* **467**, 291–296.
- Philpott, C.C. (2012). Coming into view: eukaryotic iron chaperones and intracellular iron delivery. *J. Biol. Chem.* **287**, 13518–13523.
- Plovanich, M., Bogorad, R.L., Sancak, Y., Kamer, K.J., Strittmatter, L., Li, A.A., Girgis, H.S., Kuchimanchi, S., De Groot, J., Speciner, L., et al. (2013). MICU2, a paralog of MICU1, resides within the mitochondrial uniporter complex to regulate calcium handling. *PLoS One* **8**, e55785.
- Romslo, I., and Flatmark, T. (1973). Energy-dependent accumulation of iron by isolated rat liver mitochondria. II. Relationship to the active transport of Ca^{2+} . *Biochim. Biophys. Acta* **325**, 38–46.
- Sancak, Y., Markhard, A.L., Kitami, T., Kovács-Bogdán, E., Kamer, K.J., Udeshi, N.D., Carr, S.A., Chaudhuri, D., Clapham, D.E., Li, A.A., et al. (2013). EMRE is an essential component of the mitochondrial calcium uniporter complex. *Science* **342**, 1379–1382.
- Saris, N.-E. (2012). Mitochondrial uptake of Ca^{2+} and other bivalent cations. *Biochem. Anal. Biochem.* **1**, 112.
- Schreiner, B., Westerburg, H., Forne, I., Imhof, A., Neupert, W., and Mokranjac, D. (2012). Role of the AAA protease Yme1 in folding of proteins in the intermembrane space of mitochondria. *Mol. Biol. Cell* **23**, 4335–4346.
- Senguen, F.T., and Grabarek, Z. (2012). X-ray structures of magnesium and manganese complexes with the N-terminal domain of calmodulin: insights into the mechanism and specificity of metal ion binding to an EF-hand. *Biochemistry* **51**, 6182–6194.
- Shirran, S.L., and Barran, P.E. (2009). The use of ESI-MS to probe the binding of divalent cations to calmodulin. *J. Am. Soc. Mass Spectrom.* **20**, 1159–1171.
- Sikorski, R.S., and Hieter, P. (1989). A system of shuttle vectors and yeast host strains designed for efficient manipulation of DNA in *Saccharomyces cerevisiae*. *Genetics* **122**, 19–27.

- Smith, M.R., Fernandes, J., Go, Y.M., and Jones, D.P. (2017). Redox dynamics of manganese as a mitochondrial life-death switch. *Biochem. Biophys. Res. Commun.* *482*, 388–398.
- Song, J., Liu, X., Zhai, P., Huang, J., and Lu, L. (2016). A putative mitochondrial calcium uniporter in *A. fumigatus* contributes to mitochondrial Ca²⁺ homeostasis and stress responses. *Fungal Genet. Biol.* *94*, 15–22.
- Tai, Y.K., Chew, K.C., Tan, B.W., Lim, K.L., and Soong, T.W. (2016). Iron mitigates DMT1-mediated manganese cytotoxicity via the ASK1-JNK signaling axis: implications of iron supplementation for manganese toxicity. *Sci. Rep.* *6*, 21113.
- Vasington, F.D., and Murphy, J.V. (1962). Ca ion uptake by rat kidney mitochondria and its dependence on respiration and phosphorylation. *J. Biol. Chem.* *237*, 2670–2677.
- Vecellio Reane, D., Vallese, F., Checchetto, V., Acquasaliente, L., Butera, G., De Filippis, V., Szabò, I., Zanotti, G., Rizzuto, R., and Raffaello, A. (2016). A MICU1 splice variant confers high sensitivity to the mitochondrial Ca²⁺ uptake machinery of skeletal muscle. *Mol. Cell* *64*, 760–773.
- Vinogradov, A., and Scarpa, A. (1973). The initial velocities of calcium uptake by rat liver mitochondria. *J. Biol. Chem.* *248*, 5527–5531.
- Wettmarshausen, J., and Perocchi, F. (2017). Isolation of functional mitochondria from cultured cells and mouse tissues. *Methods Mol. Biol.* *1567*, 15–32.
- Wysocki, R., and Tamás, M.J. (2010). How *Saccharomyces cerevisiae* copes with toxic metals and metalloids. *FEMS Microbiol. Rev.* *34*, 925–951.
- Yamamoto, T., Yamagoshi, R., Harada, K., Kawano, M., Minami, N., Ido, Y., Kuwahara, K., Fujita, A., Ozono, M., Watanabe, A., et al. (2016). Analysis of the structure and function of EMRE in a yeast expression system. *Biochim. Biophys. Acta* *1857*, 831–839.
- Yoo, J., Wu, M., Yin, Y., Herzik, M.A., Jr., Lander, G.C., and Lee, S.Y. (2018). Cryo-EM structure of a mitochondrial calcium uniporter. *Science* *361*, 506–511.

STAR★METHODS

KEY RESOURCES TABLE

REAGENT or RESOURCE	SOURCE	IDENTIFIER
Antibodies		
Rabbit polyclonal anti-MCU	Sigma-Aldrich	Cat#HPA016480; Lot#C0114358; RRID: AB_2071893
Rabbit polyclonal anti-EMRE - C22orf32 (clone C-12)	Santa Cruz Biotechnology	Cat#sc-86337; Lot#K0215; RRID: AB_2250685
Mouse monoclonal anti-Aequorin (clone 6E3.2)	Merck/Millipore	Cat#MAB4405; RRID: AB_94900; RRID: AB_94900
Rabbit polyclonal anti-MICU1	Sigma-Aldrich	Cat#HPA037480; Lot#N107141; RRID: AB_10696934
Anti-Sc-Yme1 produced in rabbit	Schreiner et al., 2012	N/A
Mouse monoclonal anti-TIM23	BD Bioscience	Cat#611222; Lot#3067849; RRID: AB_398754
Rabbit polyclonal anti-MICU1	Atlas Antibody	Cat#HPA037479; Lot#R34024; RRID: AB_2675495
Mouse monoclonal anti-Cyclophilin D [E11AE12BD4]	Abcam	Cat#ab110324; Lot#GR134866-15; RRID: AB_10864110
Mouse monoclonal anti-ATP5A	Invitrogen	Cat#43-9800; Lot#TA2516391; RRID: AB_2533548
Mouse monoclonal anti-V5	Life Technologies	Cat#R96025; Lot#1792242; RRID: AB_2556564
Mouse monoclonal anti-HSP60	R&D System	Cat#MAB1800; Lot#UNG02; RRID: AB_11212084
Mouse monoclonal anti-TOMM20	Abcam	Cat#Ab56783; Lot#GR3188177-1; RRID: AB_945896
Mouse monoclonal anti-β-Actin	Sigma-Aldrich	Cat#A2228; Lot#085M4754V; RRID: AB_476697
Chemicals, Peptides, and Recombinant Proteins		
Amiodarone hydrochloride	Sigma-Aldrich	Cat#A8423; CAS: 19774-82-4
Antioxidant Supplement (1000 ×)	Sigma-Aldrich	Cat#A1345
Calcium chloride dihydrate	Merck/Millipore	Cat#208290; CAS: 10035-04-8
Calcium Green-5N, Hexapotassium Salt, cell impermeant	Thermo Fisher Scientific	Cat#C3737; CAS: 153130-66-6
CM-H2DCFDA (General Oxidative Stress Indicator)	Thermo Fisher Scientific	Cat#C6827
Coelenterazine, native	Abcam	Cat#ab145165; CAS: 55779-48-1
Copper(II) chloride	Sigma-Aldrich	Cat#751944; CAS: 7447-39-4
Digitonin	Sigma-Aldrich	Cat#D141; CAS: 11024-24-1
Hydrogen peroxide 30% (w/w) solution	Sigma-Aldrich	Cat#H1009; CAS: 7722-84-1
Idebenone	Santhera Pharmaceuticals	CAS: 58186-27-9; Lot#99826G001B
Iron(II) chloride tetrahydrate	Merck/Millipore	Cat#1038610250; CAS: 13478-10-9
L-Glutathione reduced	Sigma-Aldrich	Cat#G6013; CAS: 70-18-8
Mn ²⁺ (II) chloride tetrahydrate	Merck/Millipore	Cat#1059271000; CAS: 13446-34-9
Miconazole nitrate salt	Sigma-Aldrich	Cat#M3512; CAS: 22832-87-7
N-Acetyl-L-cysteine	Sigma-Aldrich	Cat#A9165; CAS: 616-91-1
Native Mark Unstained Protein Standard-5	Life Technologies	Cat#LC0725
Native PAGE 20x Cathode Buffer	Life Technologies	Cat#BN2002
Native PAGE Novex 3-12%, Bis-Tris Protein, 10well	Life Technologies	Cat#BN1001
Native PAGE Running Buffer (20x)	Life Technologies	Cat#BN2001
NativePAGE 5% G-250 Sample Additive	Life Technologies	Cat#BN2004
NativePAGE Sample Buffer (4x)	Life Technologies	Cat#BN2003
Ru360	Calbiochem	Cat#557440
Strontium chloride hexahydrate	Merck/Millipore	Cat#1078650250; CAS: 10025-70-4
Thiazolyl Blue Tetrazolium Bromide (MTT)	Sigma-Aldrich	Cat#M5655; CAS: 298-93-1
Zinc chloride	Sigma-Aldrich	Cat#Z0152; CAS: 7646-85-7
Zymolyase 20T from <i>Arthrobacter luteus</i>	Amsbio	Cat#120491-1
6-Hydroxy-2,5,7,8-tetramethylchromane-2-carboxylic acid (Trolox)	Sigma-Aldrich	Cat#238813; CAS: 53188-07-1

(Continued on next page)

Continued		
REAGENT or RESOURCE	SOURCE	IDENTIFIER
Ruthenium Red	Sigma	R2751
Fura-2 low affinity (AM)	Teflabs	0-136
Thapsigargin	Enzo Life Sciences	BML-PE180-0005
CGP-37157	Enzo Life Sciences	BML-CM119-0005
Lipofectamine 3000	Life Technologies	L3000008
Critical Commercial Assays		
Pierce BCA Protein Assay Kit	Thermo Fisher Scientific	Cat#23227
CyQUANT Cell Proliferation Assay Kit	Thermo Fisher Scientific	Cat#C7026
Experimental Models: Cell Lines		
HEK293T cells	ATCC	CRL-11268
MICU1-knockout HEK293T cells (MICU1-KO)	Vamsi K. Mootha Laboratory	Kamer and Mootha (2014) ; Kamer et al. (2017)
MICU1-KO HEK293T cells rescued with WT MICU1	This paper	N/A
MICU1-knockout HEK293T cells rescued with EF-hands mutant MICU1	This paper	N/A
pLKO HeLa cells stably expressing WT mt-AEQ	This paper	N/A
shMCU HeLa cells stably expressing WT mt-AEQ	This paper	N/A
shMCU HeLa cells stably expressing WT mt-AEQ + HsMCU	This paper	N/A
shMCU HeLa cells stably expressing WT mt-AEQ + HsMTS ^{Af} MCU	This paper	N/A
shMCU HeLa cells stably expressing WT mt-AEQ + AfMCU	This paper	N/A
shMCU HeLa cells stably expressing WT mt-AEQ + NcMCU	This paper	N/A
shMCU HeLa cells stably expressing WT mt-AEQ + HsMTS ^{Nc} MCU	This paper	N/A
Experimental Models: Organisms/Strains		
<i>S. cerevisiae</i> : Strain background: YPH499 expressing HsMCU + HsEMRE + WT mt-AEQ	Arduino et al., 2017	N/A
<i>S. cerevisiae</i> : Strain background: YPH499 expressing HsMCU _{E264A} + HsEMRE + WT mt-AEQ	This paper	N/A
<i>S. cerevisiae</i> : Strain background: YPH499 expressing HsMCU _{D261A} + HsEMRE + WT mt-AEQ	This paper	N/A
<i>S. cerevisiae</i> : Strain background: YPH499 expressing HsMCU + WT mt-AEQ	This paper	N/A
<i>S. cerevisiae</i> : Strain background: YPH499 expressing DdMCU + WT mt-AEQ	This paper	N/A
<i>S. cerevisiae</i> : Strain background: YPH499 expressing AfMCU + WT mt-AEQ	This paper	N/A
<i>S. cerevisiae</i> : Strain background: YPH499 expressing NcMCU + WT mt-AEQ	This paper	N/A
<i>S. cerevisiae</i> : Strain background: YPH499 expressing HsEMRE + WT mt-AEQ	This paper	N/A
<i>S. cerevisiae</i> : Strain background: YPH499 expressing HsMCU + HsEMRE + HsMICU1 + WT mt-AEQ	This paper	N/A
<i>S. cerevisiae</i> : Strain background: YPH499 expressing HsMCU + HsEMRE + HsMICU1 _{mEF} + WT mt-AEQ	This paper	N/A
<i>S. cerevisiae</i> : Strain background: YPH499 + p414GPD expressing HsMCU + HsEMRE + WT mt-AEQ	This paper	N/A

(Continued on next page)

Continued

REAGENT or RESOURCE	SOURCE	IDENTIFIER
<i>S. cerevisiae</i> : Strain background: YPH499 +p423GPD + p425GPD expressing WT mt-AEQ	This paper	N/A
<i>S. cerevisiae</i> : Strain background: YPH499 expressing WT mt-AEQ	This paper	N/A
Oligonucleotides		
MCU shRNA targeting sequence: 5'-GCAAGGAGTTTCTTCTTT-3'	RNAi Consortium, Broad Institute	TRCN0000133861
Recombinant DNA		
p316GPD (plasmid)	Arduino et al., 2017	N/A
p423GPD (plasmid)	Mumberg et al., 1995	N/A
p425GPD (plasmid)	Mumberg et al., 1995	N/A
p414GPD (plasmid)	Mumberg et al., 1995	N/A
MCU full-length with V5-tag (pLX304)	Arduino et al., 2017	N/A
AfMCU full-length with V5-tag (pLX304)	This paper	N/A
^{HsMTS} AfMCU full-length with V5-tag (pLX304)	This paper	N/A
^{HsMTS} NcMCU full-length with V5-tag (pLX304)	This paper	N/A
NcMCU full-length with V5-tag (pLX304)	This paper	N/A
DdMCU full-length with V5-tag (pLX304)	This paper	N/A
MCU full-length with V5-tag (p423GPD)	Arduino et al., 2017	N/A
AfMCU full-length with V5-tag (p423GPD)	This paper	N/A
NcMCU full-length with V5-tag (p423GPD)	This paper	N/A
DdMCU full-length with V5-tag (p423GPD)	This paper	N/A
pcDNA-dest40-MICU1-HA	Kamer et al., 2017	N/A
Software and Algorithms		
GraphPad Prism 5.0 or newer	GraphPad Software	N/A
MATLAB R2014b	MathWorks	N/A
ProtPhylo	Cheng and Perocchi, 2015	www.protphylo.org
Phylogenetic tree generator	N/A	https://phylo.t.biobyte.de/
iTOL	N/A	https://itol.embl.de/
Canvas X	N/A	N/A
SigmaPlot 12.5	N/A	N/A

CONTACT FOR REAGENT AND RESOURCE SHARING

Further information and requests for resources and reagents should be directed to and will be fulfilled by the Lead Contact, Fabiana Perocchi (fabiana.perocchi@helmholtz-muenchen.de).

EXPERIMENTAL MODEL AND SUBJECT DETAILS

Cell lines

All mammalian cells were grown in high-glucose Dulbecco's modified Eagle's medium (DMEM) (Sigma-Aldrich; D6429) supplemented with 10% FBS (Sigma-Aldrich, F7524) at 37°C and 5% CO₂. HeLa cells stably expressing a WT mitochondrial matrix-targeted GFP-aequorin (mt-AEQ HeLa) were generated as previously described ([Arduino et al., 2017](#)) and selected with 100 μg/ml geneticin (Thermo Fisher Scientific, 10131027). Mt-AEQ HeLa cells stably expressing either an empty vector (pLKO; Addgene, 8453) or a pLKO vector expressing a shRNA targeting Hs-MCU (shMCU; Sigma Aldrich, TRCN0000133861) were generated as previously described ([Baughman et al., 2011](#)) and selected with 2 μg/mL puromycin (Life Technologies, A11138) and 100 μg/ml geneticin. MCU-knockdown mtAEQ HeLa cells stably expressing Hs-MCU, Nc-MCU, Af-MCU, ^{HsMTS}Af-MCU and ^{HsMTS}Nc-MCU from the pLX304 lentiviral vector were generated by transduction. Lentivirus production and infection were performed according to guidelines from the Broad RNAi Consortium and infected cell lines were selected 48 hr post-transduction with the respective selection markers. MICU1-knockout HEK293 cells were kindly provided by Prof. Vamsi Mootha (Howard Hughes Medical Institute). MICU1-knockout

HEK293 cells stably expressing either wild-type (Hs-MICU1) or mutant Hs-MICU1 (Hs-MICU1_{mEF}) from the pLX304 vector were generated by transduction and selected with 10 µg/mL blasticidin.

Yeast Strains

Yeast strains expressing mt-AEQ or cyt-AEQ were generated by transforming the wild-type yeast strain YPH499 and selecting transformants in glucose medium lacking uracil (Sikorski and Hieter, 1989). Yeast strains expressing Dd-MCU, Af-MCU, Nc-MCU, Hs-EMRE, Hs-MCU, Hs-MICU1 and their mutants were generated by transforming the YPH499 strain with the respective plasmids and by selecting transformants on glucose medium lacking uracil (empty vector p316GPD or mt-AEQ and cyt-AEQ), histidine (empty vector p423GPD or Hs-MCU, Hs-MCU_{D261A}, Hs-MCU_{E264A}, Dd-MCU, Af-MCU, and Nc-MCU), leucine (empty vector p425GPD or Hs-EMRE), and tryptophan (empty vector p414GPD or Hs-MICU1, Hs-MICU1_{mEF}) as selection markers.

METHOD DETAILS

Phylogenetic Profiling of MICU1 and MCU

Homologs of human MCU and MICU1 across 247 eukaryotes were retrieved from ProtPhylo (www.protphylo.org) (Cheng and Perocchi, 2015) using OrthoMCL with more than 0% match length and inflation index of 1.1 for orthology assignment. The percentage of amino acids match length was determined based on BLASTp-NIH. The phylogenetic tree of 247 eukaryotes was reconstructed using the phylogenetic tree generator (<https://phylot.biobyte.de/>) and visualized using iTOL (<https://itol.embl.de/>). The mitochondrial-targeting sequence (MTS) probability was determined with MitoProt (<https://ihg.gsf.de/ihg/mitoprot.html>).

Protein Domains

Protein sequences of *Homo sapiens* MCU (Hs-MCU, NP_612366.1) *Neurospora crassa* MCU (Nc-MCU, XP_959658.1), and *Aspergillus fumigatus* MCU (Af-MCU, XP_751795.1) were analyzed to predict MTS, DUF607 motif, coiled coil domains (CCD) (https://embnet.vital-it.ch/software/COILS_form.html), and transmembrane domains (TM) (TMHMM 2.0). Clustal Omega was used for proteins alignment and sequence similarities above 80% were color-coded with the Sequence Manipulation Suite tool.

Plasmids and Reagents

The lentiviral vector pLX304 was obtained from the Broad Institute's RNAi Consortium and used for expressing V5- tagged cDNAs. Full-length, human wild-type EMRE (Hs-EMRE), MCU (Hs-MCU), MICU1 (Hs-MICU1) and their mutants (Hs-MCU_{D261A}, Hs-MCU_{E264A}, and Hs-MICU1_{mEF}) cDNAs without a stop codon were obtained from Addgene. Hs-MICU1_{mEF} contains two point mutations in both first (D231A, E242K) and second (D421A, E432K) EF-hand domains as described in (Perocchi et al., 2010).

Dd-MCU, Af-MCU and Nc-MCU with (^{HsMTS}Af-MCU and ^{HsMTS}Nc-MCU) and without the N-terminal MTS of Hs-MCU (aminoacids 1-56) and without a stop codon were codon optimized for human expression, synthesized *de novo* in the PuC57 vector (GenScript) and amplified with flanked *attB1* and *attB2* sites by PCR using the following primers: fw-DdMCU (5'-GGG GAC AAG TTT GTA CAA AAA AGC AGG CTT AGC CAC CAT GAA CTC CTT TGT CAT CAG-3'); rv-DdMCU (5'-GGG GAC AAG TTT GTA CAA AAA AGC AGG CTT AGC CAC CAT GAA TTG CGT GAG AAT GAG ACT C-3'); fw-NcMCU (5'-GGG GAC AGG TTT GTA CAA AAA AGC AGG CTT AGC CAC CAT GAA TTG CGT GAG AAT GAG ACT C-3'); rv-NcMCU (5'-GGG GAC CAC TTT GTA CAA GAA AGC TGG GTT ACT GTC TCC GCT GGT CTC TTT-3'); fw-AfMCU (5'-GGG GAC AAG TTT GTA CAA AAA AGC AGG CTT AGC CAC CAT GGT CCT GTC TTG TGA TAC TAG A-3'); rv-AfMCU (5'-GGG GAC CAC TTT GTA CAA GAA AGC TGG GTT GTC GTC ATC TCG GTC ATC GTT-3'); fw-HsMTS (5'-GGG GAC AAG TTT GTA CAA AAA AGC AGG CTT AGC CAC CAT GGC GGC CGC AGG TAG A-3'). PCR products were integrated into the pDONR221 vector using a site-specific recombination system (GATEWAY cloning technology) according to manufacturer's instructions (Life Technologies). For the expression in mammalian cells, cDNAs were integrated from the pDONR221 Gateway vector (Thermo Fisher Scientific, 1253607), by site-specific recombination, into the pLX304 vector according to manufacturer's instructions (Life Technologies).

Cytosolic aequorin (cyt-AEQ) plasmid was kindly provided by Prof. Teresa Alonso (University Valladolid) and a mitochondria-targeted GFP-aequorin (mt-AEQ) plasmid was generated as previously described in (Arduino et al., 2017). cDNAs of Dd-MCU, Af-MCU, Nc-MCU, Hs-EMRE, Hs-MCU, Hs-MICU1 and their mutants were amplified by PCR using the following primers: fw-DdMCU (5'-CCC TCT AGA ATG AAC TCC TTT GTC ATC AG-3'); fw-AfMCU (5'-CCC TCT AGA ATG GTC CTG TCT TGT GAT AC-3'); fw-NcMCU (5'-CCC TCT AGA ATG AAT TGC GTG AGA ATG AG-3'); rv-V5 (5'-GGG CTC GAG CTA CGT AGA ATC GAG ACC GAG-3'); fw-HsEMRE (5'-CCC GGA TCC ATG GCG TCC GGA GCG GCT CGC-3'); rv-HsEMRE (5'-GGG CTC GAG TTA GTC ATC ATC ATC ATC CTC-3'); fw-HsMCU (5'-CCC TCT AGA ATG GCG GCC GCC GCA GGT AG-3'); rv-HsMCU (5'-GGG CTC GAG TTA ATC TTT TTC ACC AAT TTG TCG-3'); fw-HsMICU1 (5'-CCC GGA TCC ATG TTT CGT CTG AAC TCA CTT TC-3'); rv-HsMICU1 (5'-GGG CTC GAG TTA CTG TTT GGG TAA AGC GAA G-3'), and cloned into the yeast expression plasmids p423GPD (Dd-MCU, Af-MCU, Nc-MCU, Hs-MCU, Hs-MCU_{D261A}, Hs-MCU_{E264A}), p414GPD (Hs-MICU1, Hs-MICU1_{mEF}) and p425GPD (Hs-EMRE) as in (Mumberg et al., 1995).

Isolation of Crude Mitochondria from HeLa Cells

Crude mitochondria were prepared from cultured HeLa cells as previously described (Wettmarshausen and Perocchi, 2017). Briefly, HeLa cells were grown to confluency in 245 × 245 × 20 mm cell culture plates. Culture medium was removed and cells were rinsed

with 30 mL PBS, scraped down and resuspended in 5 mL PBS. After 5 minutes of centrifugation at 600 x g, 4°C, the cell pellet was resuspended in ~15 mL of ice cold isolation buffer (IB; 220 mM mannitol, 70 mM sucrose, 5 mM HEPES-KOH pH 7.4, 1 mM EGTA-KOH pH 7.4), with one protease inhibitor tablet added per 50 mL of buffer. Cell suspension was immediately subjected to nitrogen cavitation at 600 psi for 10 minutes at 4°C. Nuclei and intact cells were pelleted by centrifugation at 600 x g for 10 minutes at 4°C. Supernatants were transferred into new tubes and centrifuged at 8000 x g for 10 minutes at 4°C. The resulting pellet containing crude mitochondria was resuspended in 50-200 μ l IB for further analyses.

Topology Analysis of Mitochondrial Proteins

Alkaline carbonate extraction from crude mitochondria was performed as described previously (Baughman et al., 2011). Briefly, 100 μ g of mitochondria were pelleted by centrifugation at 8000 x g for 10 minutes at 4°C. Pellets were resuspended in 0.1 M Na₂CO₃ at pH 10, pH 11 or pH 12 and incubated for 30 minutes on ice. Samples were then centrifuged at 45,000 x g for 10 minutes at 4°C. Pellets were resuspended in 100 μ l of 2 x Laemmli buffer, boiled at 98°C for 5 minutes and stored at -80°C until further use (pellet sample). Supernatants were mixed with 40 μ l of 100% TCA and incubated overnight at -20°C. On the following day, supernatants were centrifuged at 16,000 x g for 25 min at 4°C. Pellets were then washed twice with cold acetone, air-dried for 20-30 minutes at room temperature, resuspended in 100 μ l of 2 x Laemmli buffer and heated up to 98°C for 5 minutes (supernatant sample). 25 μ l of supernatant and pellet samples were analyzed by SDS-PAGE. TIM23 and HSP60, integral inner membrane and soluble matrix targeted proteins, respectively, are used as controls.

Proteinase K protection assay was performed by incubating 30 μ g of mitochondria in 30 μ l of isolation buffer with increasing concentrations of digitonin or 1% Triton X-100 in the presence of 100 μ g/ml proteinase K to sequentially permeabilize outer and inner membranes. The reaction was carried out at room temperature for 15 minutes and was stopped by the addition of 5 mM PMSF, followed by incubation on ice for 10 minutes. Samples were mixed with 10 μ l of 4 X Laemmli buffer containing 10% 2-mercaptoethanol and boiled for 5 minutes at 98°C. Samples were then loaded at 10 μ l per lane and were analyzed by SDS-PAGE. TOM20 and cyclophilin D (Cyp D), an integral outer membrane and a soluble matrix protein, respectively, were used as controls.

Blue Native - PAGE Analysis

Samples for BN-PAGE analysis were prepared by incubating 10 μ g of crude mitochondria on ice for 10 minutes in 9.5 μ l of Invitrogen 1X NativePAGE™ sample buffer containing 1% digitonin. Samples were centrifuged at 20,000 x g for 30 minutes at 4°C. Supernatants were transferred into new tubes and 0.5 μ l of NativePAGE™ 5% G-250 Sample Additive was added to a final concentration of 0.25%. Anode and cathode buffers for gel electrophoresis were prepared according to the manufacturer's protocol for the Invitrogen NativePAGE™ Novex® Bis-Tris Gel System and were cooled to 4°C before use. Electrophoresis was performed at 4°C and gels were performed at 40 V for 1 hour. The voltage was then increased to 60 V for 30 minutes and subsequently to 100 V until the dye front had traveled through 1/3 of the gel, at which point the Dark Blue Cathode Buffer was replaced with Light Blue Cathode Buffer. Electrophoresis was continued at 100 V for 30 minutes and then increased to 150 V until completed. Proteins were transferred onto PVDF membranes by electrophoretic wet transfer overnight at 40 V, 4°C. After transfer, proteins were fixed on the membrane by incubating in 8% acetic acid for 15 minutes at room temperature on a shaker. Immunoblot analyses were performed with the following antibodies: anti-MCU (Sigma Aldrich, HPA01648), anti-V5 (Life Technologies, R96025), and anti-ATP5A (Abcam, MS507), anti-TIM23 (BD Bioscience, 611222), and anti-HSP60 (R&D System, MAB1800), anti-TOM20 (Abcam, ab56783), and anti-Cyclophilin D (Abcam, ab110324).

Measurements of Mitochondrial Calcium Uptake in Intact HeLa Cells

Mitochondrial Ca²⁺ uptake was measured in mt-AEQ HeLa cells as previously described (Arduino et al., 2017). Briefly, HeLa cells stably expressing mt-AEQ were seeded in white 96-well plates at 25,000 cells/well in growth medium. After 24 hours, mt-AEQ was reconstituted with 2 μ M native coelenterazine (Abcam, ab145165) for 2 hours at 37°C. Mt-AEQ-based measurements of Ca²⁺-dependent light kinetics were performed upon 100 μ M histamine stimulation. Light emission was measured in a luminescence counter (MicroBeta2 LumiJET Microplate Counter, PerkinElmer) at 469 nm every 0.1 s. At the end of each experiment, cells were lysed with a solution containing 0.5% Triton X-100 and 10 mM CaCl₂ to release all the residual aequorin counts.

Measurements of Mitochondrial Calcium Uptake in Digitonin-Permeabilized HeLa Cells

HeLa cells stably expressing mt-AEQ were harvested at a density of 500,000 cells/mL in growth medium supplemented with 20 mM HEPES (pH 7.4/NaOH) and the photoprotein aequorin was reconstituted by incubation with 3 μ M native coelenterazine for 2.5 hours at room temperature. Cells were then centrifuged at 300 g for 3 minutes and the pellet was re-suspended in an extracellular-like buffer containing 145 mM NaCl, 5 mM KCl, 1 mM MgCl₂, 10 mM glucose, 10 mM HEPES and 500 μ M EGTA (pH 7.4/NaOH), supplemented with 200 nM thapsigargin. After 20 minutes at room temperature, cells were collected by centrifugation at 300 g for 3 minutes and the pellet was resuspended in an intracellular-like buffer containing 140 mM KCl, 1 mM KH₂PO₄/K₂HPO₄, 1 mM MgCl₂, 20 mM HEPES, 100 μ M EGTA (pH 7.2/KOH), supplemented with 1 mM Na⁺-pyruvate, 1 mM ATP/MgCl₂ and 2 mM Na⁺-succinate. Cells were permeabilized with 60 μ M digitonin for 5 minutes, collected by centrifugation at 300 g for 3 minutes and resuspended in intracellular-like buffer at a density of ~900 cells/ μ L. Then, 90 μ L of cell suspension was dispensed into a white 96-well plate (PerkinElmer). Cells were incubated for 5 minutes at room temperature and Ca²⁺-stimulated light signal was recorded at 469 nm every 0.1 s using a luminescence counter (MicroBeta2 LumiJET Microplate Counter, PerkinElmer). Ru360 (10 μ M) was used as a positive control.

Subcellular Fractionation of Yeast Cells

To test the expression and subcellular localization of heterologous proteins, yeast cells were grown at 30°C in a selective lactate medium (S-LAC) containing 8.5 g/L yeast nitrogen base, 25 g/L ammonium sulfate, 2% (v/v) lactic acid (90%), 0.1% glucose (pH 5.5/KOH), supplemented with the respective selection markers. At an OD ~0.8, cells were harvested at 1000 g for 5 minutes at room temperature. The cell pellet was re-suspended in SHK buffer (0.6 M sorbitol, 20 mM HEPES/KOH pH 7.2, 80 mM KCl, and 1 mM PMSF) and vortexed five times for 30 s with glass beads (425–600 μm diameter), with a 30 s cooling interval in between. This sample was then centrifuged at 1000 g for 5 minutes at 4°C and the supernatant was further centrifuged at 20,000 g for 10 minutes at 4°C to obtain the mitochondrial fraction (pellet). The resulting supernatant (cytosolic fraction) was precipitated with trichloroacetic acid at –20°C for 1 hour, washed once with cold acetone and centrifuged at 20,000 g for 10 minutes at 4°C to obtain the cytosolic fraction (pellet). Both cytosolic and mitochondrial fractions were directly resuspended in Laemmli buffer and separated under reducing conditions in 12 or 14% SDS-PAGE gels. Immunoblotting was performed according to the standard procedures using the following antibodies: anti-MCU (Sigma-Aldrich, HPA016480); anti-EMRE (Santa Cruz Biotechnology, sc- 86337); anti-MICU1 (Sigma Aldrich, HPA037480); anti-YME1 (ThermoFisher/Novex, 459250); anti-AEQ (Merck/Millipore, MAB4405).

Measurements of Calcium Transients in Intact Yeast Cells

In vivo analyses of cytosolic and mitochondrial Ca²⁺ dynamics in yeast cells were performed as described by (Groppi et al., 2011) with some modifications. Yeast were grown in S-LAC at 30°C overnight to an OD ~0.8, (~24x10⁶ cells/mL), and cells were harvested by centrifugation at 3,500 g for 5 minutes at room temperature. Yeast cell pellet was washed three times with milliQ water and resuspended in a nutrient-free buffer (NFB; 100 mM Tris, pH 6.5) at a density of 1x10⁸ cells/mL. Cells were incubated for 1.5 hours at room temperature (starvation), collected by centrifugation at 3,500 rpm for 5 minutes and concentrated in the same buffer to a density of 25x10⁸ cells/mL. The photoprotein aequorin was then reconstituted with 50 μM native coelenterazine in the dark for 30 minutes at room temperature. Excess of coelenterazine was washed thrice with NFB and the cell pellet was resuspended to a final density of 5x10⁸ cells/mL. Then, a suspension of 0.5x10⁸ cells/well were plated into a white 96-well plate and Ca²⁺-dependent aequorin light signal was recorded upon stimulation with containing 1 mM CaCl₂ and 100 mM glucose, at 0.5 s interval in a MicroBeta2 LumiJET Microplate Counter. At the end of each experiment, a lysis solution containing 5 mM digitonin, 450 mM EGTA, 100 mM Tris (pH 6.5/KOH) was added at a ratio of 1:5 for 5 minutes at 37°C and light response was measured upon the addition of CaCl₂ to a final concentration of 140 mM to release all the residual aequorin counts.

Measurements of Mitochondrial Calcium Uptake in Isolated Yeast Mitochondria

Crude mitochondria were isolated from yeast strains as described previously (Arduino et al., 2017). Mitochondria were then resuspended in a buffer containing 0.6 M sorbitol, 20 mM HEPES, 2 mM MgCl₂, 10 mM KH₂PO₄, 3 mM glutamate, 3 mM malate, 3 mM succinate, 50 μM EDTA, and 0.1 μM Calcium Green-5N (Life technologies, C3737) and seeded into a black 96-well plate at 150 μg/100 μL. Calcium Green-5N fluorescence (excitation 506 nm, emission 531 nm) was monitored every 2 s at room temperature using a CLARIOstar microplate reader (BMG Labtech Perkin-Elmer Envision) after injection of CaCl₂ (100 μM final concentration). The MCU inhibitor Ru360 (10 μM) was used as a positive control.

Yeast Growth Measurement

For growth assays in liquid media, overnight yeast cultures grown at 30°C in S-LAC were diluted to an OD of 0.1 (3x10⁶ cells/mL) and then 0.3x10⁶ cells/well were seeded in a black, gas-permeable Lumox 96-well plate. Absorbance measurements of yeast suspension light scattering were performed at λ_{max} = 600 nm and intervals of 340 s using a CLARIOstar microplate reader (BMG Labtech) for 48–72 hours with shaking at 30°C, 37°C, or in the presence of sterile solutions of sodium chloride (NaCl, 0.1–1 M), calcium chloride (CaCl₂, 10–100 mM), copper (II) chloride (CuCl₂, 10–30 mM), iron (II) chloride (FeCl₂, 10–40 mM), Mn²⁺ (II) chloride (MnCl₂, 1–5 mM), strontium (II) chloride (SrCl₂, 10–50 mM), zinc (II) chloride (ZnCl₂, 10–50 mM), or antifungal drugs (miconazole, 10–100 ng/ml; amiodarone, 5–20 μM). The average time taken by the yeast culture to double in the log-growth phase (doubling time) was calculated using the following equation:

$$\text{Doubling time} = \frac{(T_f - T_i) * \log(2)}{\log(N_f) - \log(N_i)}$$

where T is the time between the log-growth phase from T_i to T_f and N the number of cells measured as an optical density at λ_{max} = 600 nm at the time point T_i (N_i) and T_f (N_f).

For spot assays, yeast cultures grown at 30°C in S-LAC were harvested at an OD of 1.0 (30x10⁶ cells/mL) at 3200 g for 5 minutes at room temperature. The cell pellet was re-suspended in sterile water to 30x10⁶ cells/mL and diluted in a 10-fold series. Aliquots of 5 μL from each dilution were spotted onto a S-LAC plate with or without the respective treatment (CaCl₂, 100–600 mM; SrCl₂, 50–500 mM). Plates were then incubated at 30°C for 72 h.

Cell Viability Analysis

A colorimetric 3-(4,5-dimethylthiazol-2-yl)-2,5-diphenyltetrazolium bromide (MTT) metabolic activity assay was used to determine cell viability. HEK293 cells were seeded at 50,000 cells/well in 1 mL of DMEM with high glucose and 10% FBS in a transparent

24-well plate at 37°C and 5% CO₂. After 24 hours, cells were incubated in the presence or absence of metal ions (FeCl₂, 0.1-1 mM; MnCl₂, 5-50 μM) or antioxidants (N-acetyl-L-cysteine, NAC, 1-10 mM; L-glutathione, GSH, 1-20 μM; antioxidant supplement, 1-20X concentration according to manufacturer's protocol; Trolox, 0.5-5 mM; Idebenone, 0.1 μM), together with 10-50 μM of MnCl₂, for further 48 hours. Afterward, 500 μL of medium was replaced, 50 μL of MTT solution (Sigma Aldrich, M5655; 5 mg/ml in PBS) was added, and cells were incubated for 3 hours at 37°C. Finally, cells were lysed with 500 μL of solubilization solution (1% SDS and 0.1 M HCl in isopropanol) for 15 minutes at 37°C and absorbance at λ_{max} 570 nm was monitored in a CLARIOstar microplate reader (BMG Labtech).

Mitochondrial Mn²⁺ Transport Measurement in Human Cells

Measurements of Mn²⁺ uptake in mitochondria were performed as previously described (Csordás and Hajnóczky, 2003). Briefly, cells were first loaded with Fura2FF/AM (4 μM for 60 min) and then rinsed with a Ca²⁺-free extracellular buffer containing 100 μM EGTA. Permeabilization was carried out in 1 mL ICM (120 mM KCl, 10 mM NaCl, 1 mM KH₂PO₄, 20 mM Tris-HEPES, 2 mM MgATP, and 1 μg/ml each of antipain, leupeptin and pepstatin at pH 7.2) supplemented with saponin (20 μg/ml) and 20 μM EGTA/Tris (pH 7.4) in the incubation chamber for 5 min (35°C). Subsequently, fresh ICM supplemented with succinate (2 mM) and CGP (20 μM) to energize mitochondria and to inhibit mitochondrial Ca²⁺ efflux, respectively. Fluorescence imaging of Fura2FF-quenching by Mn²⁺ was carried out using a multiwavelength beamsplitter/emission filter combination and a high quantum-efficiency cooled CCD camera. Fura2FF was excited at 360 nm (Mn²⁺ quench). Image analysis was performed using custom-made software (Spectralyzer). Genetic rescue of MICU1-KO HEK293 cells was performed with either WT MICU1 or pcDNA 48 hr before imaging.

ROS Measurement

HEK293 cells were loaded with 10 μM of 5-(and-6)-chloromethyl-2', 7'-dichlorodihydrofluorescein diacetate (CM-H₂DCFDA) in Krebs buffer (140 mM NaCl, 5 mM KCl, 1 mM MgCl₂, 5.6 mM D-glucose, 20 mM HEPES, 1.5 mM CaCl₂, 1 mM NaH₂PO₄, pH 7.4) for 30 minutes at 37°C. Cells were washed once with PBS, re-suspended in DMEM (without phenol red, REF, source ID), supplemented with 5 mM glucose, 1 mM pyruvate, 2 mM L-glutamine and 10% FBS, seeded at 20,000 cells/well in a black 96-well plate, and treated with 25 μM of MnCl₂ for 48 hours. H₂O₂ (50-100 μM) was used as a positive control. Fluorescence was measured at an excitation and emission wavelength of 485 nm and 520 nm respectively. Data was normalized to cell number quantified using a CyQUANT Cell Proliferation Assay Kit (Thermo Fisher Scientific).

QUANTIFICATION AND STATISTICAL ANALYSIS

Quantification of Calcium Transients

Quantification of mt-Ca₂₊ concentration was performed using a MATLAB software as previously described in (Arduino et al., 2017). The dynamics of mt-Ca²⁺-dependent luminescence signal was smoothed by the cubic spline function:

$$p \sum_1^n (y_i - f(x_i))^2 + (1 - p) \int \left(\frac{d^2 f}{dx^2} \right)^2 dx$$

Where, p is a smoothing parameter, controlling the tradeoff between fidelity to the data and roughness of the function estimate, f is the estimated cubic spline function to minimize the above function, and x_i and y_i are the dynamical data points. Here, p is set at 0.5. Parametrization of the Ca²⁺-dependent luminescence kinetics was performed in order to determine the maximal amplitude of the luminescence signal (peak) and the left slope of the bell-shaped kinetic trace. Aequorin-based luminescence signal calibration into mt-Ca²⁺ concentration was performed using the algorithm reported in (Bonora et al., 2013) for wild-type aequorin and native coelenterazine, with the following formula:

$$[Ca^{2+}] (M) = \frac{\left(\frac{L}{L_{max}} \times \lambda \right)^{\frac{1}{n}} + \left(\left(\frac{L}{L_{max}} \times \lambda \right)^{\frac{1}{n}} \times K_{TR} \right) - 1}{K_R - \left(\left(\frac{L}{L_{max}} \times \lambda \right)^{\frac{1}{n}} \times K_R \right)}$$

Where $\lambda = 1$, $K_R = 7.23 \times 10^6$, $K_{TR} = 120$ and $n = 2.99$ are the calibration values used for WT aequorin and native coelenterazine.

Data Analysis

Data are represented as mean ± SEM and the statistical analysis of each experiment is described in the figure legends including the statistical tests used and the exact value of n . Here n represents the number of biological replicates. For each biological replicate experiment at least 3 technical replicates were used for quantification and data analysis. Normal distribution was tested by Shapiro-Wilk normality test. Differences between two datasets were evaluated by two-tailed unpaired Student's t test. Statistical tests between multiple datasets and conditions were carried out using one-way analysis of variance (ANOVA) followed by Tukey's or Dunnett's Multiple Comparison tests. Statistical analyses were performed using GraphPad Prism (GraphPad Software, version 7).